

Granular hydrogel matrices with tunable plastic deformation properties for tissue engineering

James Reeves
Department of Chemical Engineering
McGill University, Montreal, Quebec, Canada

October 2022

A thesis submitted to McGill University in partial fulfillment of the requirements for the degree
of Master of Science

©James Reeves 2022

Abstract

Understanding the complex behaviour of cells in 3D culture environments requires control and knowledge of the mechanical and chemical signals they are receiving. While naturally derived hydrogels are widely used in 3D culture studies, it can be difficult to decouple the various cell to extracellular matrix (ECM) signals for understanding their individual roles. Synthetic hydrogels have been designed to study individual elastic or viscoelastic properties, but they typically do not provide plastic ECM restructuring that can be seen in their naturally derived counterparts. As such, it is not well known how plastic deformation behaviour of the ECM plays a role in 3D cell cultures as there has yet to be a platform engineered specifically for exploring this mechanical property. Packed granular hydrogels have recently become of interest for their unique characteristics, such as their self-healing and shear-thinning behaviour, providing the basis for development of new 3D culture platforms. This work presents a packed granular polyacrylamide hydrogel functionalized with guest-host chemistry, providing reversible interlinking between individual granules, allowing for a plastically deformable gel. This thesis shows that tuning of the packed gels' mechanical properties is possible via control of the individual granule characteristics. Granule size, stiffness, and levels of guest and host functionalization were varied, and rheological characterization of the gels was completed for their shear elastic moduli, measured from 70 to 960 Pa, and yield stress, spanning between 40 to 370 Pa. When applied to breast cancer aggregates, growth was observed in all conditions, with higher overall growth in gels with lower stiffness and yield stress. Cell invasion was observed for gels with lower yield stresses of 40 and 70 Pa, with lower yield leading to earlier invasion, between days 2 and 3 compared to days 3 and 4, respectively. These results indicate the potential of this platform to study the role of ECM plasticity. The proposed packed granular hydrogel begins to address the need for control over mechanical plasticity, allowing for better understanding of this property in tissue fate and function.

Résumé

Pour comprendre le comportement complexe des cellules dans les environnements de culture cellulaire en 3D, il faut contrôler et connaître les signaux mécaniques et chimiques qu'elles reçoivent. Les hydrogels d'origine naturelle sont largement utilisés dans les études de culture en 3D, par contre il peut être difficile de découpler les différents signaux entre les cellules et leur matrice extracellulaire (MEC) pour comprendre leurs rôles individuels. Les hydrogels synthétiques ont été conçus pour étudier soit les propriétés élastiques ou viscoélastiques, mais ils n'offrent généralement pas la restructuration plastique de la MEC que l'on peut observer dans leurs homologues naturels. En tant que tel, le rôle du comportement de déformation plastique de la MEC dans les cultures cellulaires en 3D demeure largement inconnu, car il n'existe pas encore de plateforme conçue spécifiquement pour explorer cette propriété mécanique. Les hydrogels granulaires ont récemment suscité l'intérêt pour leurs caractéristiques uniques, telles que leur comportement d'auto-guérison et rhéofluidifiant, fournissant une base pour le développement de nouvelles plateformes de culture 3D. Ici, ce travail présente un hydrogel de polyacrylamide à granules fonctionnalisés par une chimie hôte-invité, fournissant une liaison réversible entre les granules individuels, ce qui permet de former un gel plastiquement déformable. Cette thèse montre que le réglage des propriétés mécaniques des gels granulaires est possible via le contrôle des caractéristiques des granules individuels. Leur taille, leur rigidité et les niveaux de fonctionnalisation relatives de l'hôte et de l'invité ont été variés, et la caractérisation rhéologique des gels a été complétée pour leurs modules élastiques de cisaillement, mesurés de 70 à 960 Pa, et leur limite d'élasticité, comprise entre 40 et 370 Pa. Lorsqu'ils ont été appliqués à des agrégats de cancer du sein, une croissance a été observée sous toutes conditions, avec une croissance globale plus élevée dans les gels ayant une rigidité et une limite d'élasticité plus faibles. L'invasion cellulaire a été observée dans les gels présentant des limites d'élasticité plus faibles, de 40 à 70 Pa, dont les contraintes plus faibles entraînent une invasion plus précoce, observée aux jours 2 et 3 au lieu des jours 3 et 4 respectivement. Ces résultats indiquent le potentiel de cette plateforme pour étudier le rôle de la plasticité de la MEC. Donc, l'hydrogel granulaire proposé donne place au développement de plateforme de culture

cellulaire avec contrôle de plasticité mécanique, permettant une meilleure compréhension de cette propriété dans le sort et la fonction des tissus biologiques.

Acknowledgements

First and foremost, I would like to thank my supervisor, Professor Christopher Moraes. I am extremely grateful for your guidance, support, and feedback over the past two years. I truly believe your understanding approach as a supervisor, excitement for research, and curiosity to pursue innovative ideas allowed me to succeed and grow as a student. The skills and knowledge I have gained during my time as your student will be invaluable as I move on to my next chapter.

To all the members of the Moraes Lab, thank you for welcoming me during a particularly strange time in everyone's life. COVID made things different, but you all still made me feel like part of the lab. Ray, thanks for showing me the ropes and being patient with all my questions. Christina, this thesis would not be possible without your help and support, from cell culture to statistics, kindly helping with the abstract French translation, and all my other questions, thank you.

Ray, Steph, and Chen, thanks for being my first Montreal friends, helping me get out of my apartment, and experience the city. From the ski trip, bike rides, food, drinks, fireworks, to climbing Mont Royal, thanks. Gabe, thank you for letting me tag along to trivia, going snow shoeing, camping, and all the other OSHHH crew adventures. Camille and Christina, thank you for sharing all the lunch breaks and conversations to pass the time, you both made the long day of bead making bearable. Ben and Nick, we really only got to know each other over the past year, but I'm glad we were able to take lab breaks, play squash, hit the gym, and explore Montreal. Thank you to the whole lab for making my time here memorable, all the support with my project, and the lifelong friendships.

Finally, thank you to my parents and family for their unconditional support, especially when I told them I'm moving to the other side of Canada, and then helping me move there and back. I would not have been able to do this without you.

Contributions of Authors

The data and analysis presented in this work was obtained by the author. β -cyclodextrin-acrylamide, adamantane-acrylamide, and the β -cyclodextrin and adamantane fluorescein dyes were synthesized by Mostafa Rammal of Professor Matthew Harrington's lab. The cyclodextrin precursor reagent was synthesized by Dr. Violeta Toader. Mostafa Rammal provided written protocols of their synthesis. MCF7 and T47D cell lines and aggregates were kept in culture and provided by Christina Boghdady of Professor Christopher Moraes' Lab for use. This thesis was primarily written by the author and edited by Professor Christopher Moraes.

Table of Contents

Abstract.....	1
Résumé.....	2
Acknowledgements.....	4
Contributions of Authors	5
Table of Contents.....	6
List of Figures	8
List of Tables	9
List of Abbreviations	10
1 Introduction	11
1.1 Motivation.....	11
1.2 Aims.....	12
2 Background and Literature Review.....	13
2.1 Extracellular Matrix Elasticity and Plasticity	13
2.2 Defining and Classifying Hydrogels	16
2.3 Granular Hydrogels	19
2.4 Guest-Host Complexes.....	23
3 Approach.....	26
4 Materials and Methods.....	27
4.1 Bulk hydrogel fabrication	27
4.2 Preparation of β -cyclodextrin and adamantane acrylamides and dyes	28
4.3 Granular hydrogel fabrication and assembly.....	28
4.4 Imaging and analysis of hydrogels	29
4.5 Micromanipulation of microgels.....	30
4.6 Rheological characterization of hydrogels.....	30
4.7 Cell and aggregate culture	31
4.8 Creation of figures and statistical analysis of aggregate growth.....	33
5 Results.....	35
5.1 Fabrication of guest and host functionalized PAAm microgels	35

5.2	Confirmation of guest and host interactions	37
5.3	Repeated adhesion of Ad beads to β CD bulk gels	40
5.4	Mechanical properties of packed granular hydrogels	42
5.5	Plastically tunable granular hydrogels as an aggregate culture platform.	45
6	Discussion.....	52
7	Directions for Future Work.....	57
8	Conclusions	60
9	References	62
10	Appendix 1: Supplementary Material.....	77
10.1	Initial Ad and β CD concentration curves	77

List of Figures

Figure 1: Stiffnesses of in vivo tissues and corresponding hydrogels..	14
Figure 2: Cell functions dependent on hydrogel pores, degradability, and plasticity.	16
Figure 3: Hydrogel categorization.....	19
Figure 4: Granular hydrogel fabrication techniques.....	21
Figure 5: Inherently unique properties of granular hydrogels.	23
Figure 6: Formation of guest-host PAAm crosslinking.....	24
Figure 7: Stress-strain curve for a PAAm hydrogel with β CD and Ad crosslinking.	25
Figure 8: Granular packed hydrogel fabrication workflow.....	26
Figure 9: Granule hydrogel size as a function of vortex time.	35
Figure 10: Granule guest and host functionalization.	36
Figure 11: PAAm formulation storage modulus.	37
Figure 12: Mixing interactions of functionalized and unfunctionalized PAAm beads.....	37
Figure 13: Soft and stiff guest and host granule interactions.	39
Figure 14: Effect of mixing methods on packed gels.....	40
Figure 15: Repeatability of guest-host complex formation.....	41
Figure 16: Rheological characterization of granular packed gels.	44
Figure 17: Live/dead study of guest and host granules.....	45
Figure 18: T47D growth in TrueGel hydrogels.....	47
Figure 19: T47D growth in packed granular guest-host hydrogels.	48
Figure 20: Day 6 T47D aggregate growth.	49
Figure 21: Invasion of T47D aggregates in TrueGel hydrogels.	50
Figure 22: Invasion of T47D aggregates in packed granule guest-host hydrogels.	51
Figure 23: Initial fluorescent guest host functionalization curves for Ad and β CD.....	77

List of Tables

Table 1: PAAm gel formulations for 1000 μL of gel. From ⁶⁹	27
Table 2: Fabrication parameters used for packed granular gels in T47D aggregate cultures.....	45

List of Abbreviations

2D – Two-dimensional

3D – Three-dimensional

AAM – Acrylamide

Ad – Adamantane

APS – Ammonium persulfate

DMEM - Dulbecco's Modified Eagle's Medium

ECM – Extracellular matrix

PAAm – Polyacrylamide

PBS – Phosphate buffered saline

PEG - Polyethylene glycol

PGPR - Polyglycerol polyricinoleate

TEMED – Tetramethylethylenediamine

β CD – β -cyclodextrin

1 Introduction

1.1 Motivation

Cell and tissue models have traditionally been studied using two-dimensional (2D) culture models or within more complex animal models. These models have been crucial to biomedical advancements since their implementation, providing breakthroughs in cell signaling, behaviour, and differentiation, screening of drugs and therapeutics, or providing insight into disease progression. However, 2D and animal models have their limitations. 2D culture models lack the complex three-dimensional (3D) extracellular matrix (ECM) interactions and cell to cell interactions that can provide essential biomechanical signals, and the clinical translation of animal models to humans is often difficult due to significant differences in their anatomy and physiology¹⁻³. This has led researchers in recent years to develop more complex 3D tissue models to address these shortcomings.

A commonly used 3D culture platform is Matrigel, a naturally derived hydrogel from mouse cells, providing both mechanical and chemical signals to promote tissue growth and differentiation. While Matrigel is commonly used in stem cell and cancer studies, its batch to batch protein composition can vary up to 53% and its mechanical modulus ranges from 120 to 450 Pa leading to issues with variability and reproducibility of results in cultures^{4,5}. Additionally, it is more recently believed that plastic deformation of the ECM plays a key role in tissue function and deformation^{6,7}. While synthetic 3D culture platforms have targeted elastic and viscoelastic properties as drivers of cell behaviour, the plastic properties, and the transition from elastic to plastic deformation of the ECM is not well understood or controlled for, in the study of cell fate and function.

Therefore, the motivation behind this project was to develop and characterize a 3D cell and tissue culture platform that allows for the tuning of both its elastic storage modulus and yield point into the plastic deformation region. This system may support a transition to more mechanically and chemically stable hydrogel from the commonly used Matrigel, allowing for increased reproducibility in aggregate cultures. Additionally, a plastically tunable hydrogel would allow for

a deeper understanding of plasticity's mechanobiological role in cell behaviour, aggregate growth, organoid differentiation, and ECM-to-cell signaling.

1.2 Aims

The aim of this work was to develop an elastic and plastically tunable hydrogel system and apply it as an extracellular matrix in tissue cultures. The ability to tune the elastic to plastic deformation yield point in addition to the elastic properties of synthetic hydrogels would address problems with variability in commonly used natural systems like Matrigel, provide more homogeneous 3D culture models, and allow for a deeper understanding of how varying plasticity plays a role in tissue behaviour. This project works toward this through three specific aims as follows:

1. Develop a method to fabricate sets of microgels with either adamantane or beta-cyclodextrin moieties such that when combined, the individual microgels interlink with each other via guest-host inclusion complexes and form a packed granular hydrogel.
2. Tune and characterize the elastic and plastic properties of the packed gels through manipulation of the microgels size, stiffness, and the concentration of guest or host molecules in the pre-gel setup.
3. Characterize growth and invasion of aggregates in the packed granular gel for different elastic and plastic properties in comparison to a purely elastic platforms.

2 Background and Literature Review

2.1 Extracellular Matrix Elasticity and Plasticity

Directing cell fate and function has long been one of the goals of cell and tissue studies. This has traditionally been controlled through various soluble signals, such as growth factors, included in the media of a 2D culture. However, there has more recently been a shift to exploring the mechanisms of mechanical signals on cell behaviour, partly spurred on by the advent of 3D cell culture platforms which allows for interaction with a more complex extracellular environment. The characteristics of the 3D environment can be engineered for fine control over the signals it provides for tissue and cell behaviour⁸. It has been shown that transitioning from a 2D to a 3D culture alone can promote increased gene expression as a marker of neural differentiation⁹, or that cardiomyocyte differentiation could occur in a 3D self-assembling peptide hydrogel without the addition of ascorbic acid that is required in its 2D counterpart¹⁰. We also see that movement of cells through an ECM is influenced by its properties, such as stiffness gradients¹¹, the size of pores through the matrix¹², and even the composition, crosslinking, alignment and distribution of components in the ECM itself^{13,14}. These studies show the importance of selecting an appropriate ECM platform as it can influence cell behaviour in a variety of ways.

One of the properties of the ECM that has been shown to influence cell function, and more specifically stem cell fate decisions, is the stiffness or elastic modulus of the material chosen¹⁵. We see within the body a range of stiffness, from soft brain tissue to very stiff bone tissue, and choosing the proper 3D culture platform will influence how well we are able to study these types of tissue and provide a more accurate model as to what is seen in vivo (Figure 1)¹⁶. For example, Zoldan et al. showed that the differentiation lineage of human embryonic stem cells into ectoderm, endoderm, or mesoderm cells can be decided by the elastic modulus of the culture substrate, less than 0.1 MPa, 0.1 to 1 MPa, and 1.5 to 6 MPa respectively¹⁷. Their work also showed how too stiff of a substrate, greater than 6 MPa, led to low gene expression and kept the cells in an undifferentiated state¹⁷. Conventional 2D cell culture plastic dishes and flasks are 10 MPa, if were used instead would be well above the 6 MPa threshold for low stem cell activity. This work, among others, shows how mechanical stiffness can be a key regulator in cell function

as well as the importance of selecting a platform with appropriate mechanical properties. This type of mechanical mechanism for directing cell fate plays a role in different stem cell types and lineages, such as oligodendrocyte or neuronal differentiation for stiffer and softer ECM^{18,19}, or myogenic and osteogenic differentiation for substrate stiffness in conjunction with specific surface ECM proteins^{20,21}. It has also been shown that stiffness can be used to aid in reprogramming of cells into induced pluripotent stem cells^{22,23} and maintaining of their pluripotency state^{24,25}. This highlights the importance that ECM mechanical properties have in cell development and as a crucial tool in engineering tissues.

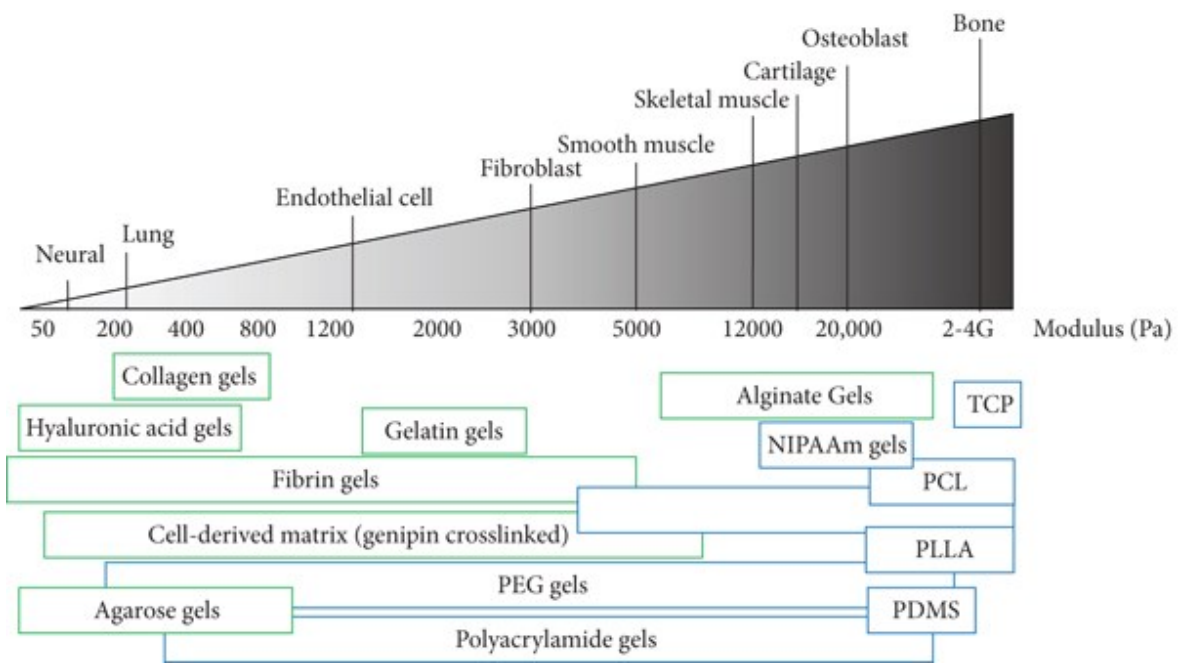


Figure 1: Stiffnesses of in vivo tissues and corresponding hydrogels. Range of stiffnesses for healthy, in vivo, tissues and the range of synthetic (blue) and naturally (green) derived hydrogel stiffnesses capable of replicating the in vivo condition. Image copyright © 2018 Taylor B. Bertucci and Guohao Dai CC BY 4.0¹⁶.

While stiffening of tissues was traditionally thought of as a consequence of disease, stiffness of the ECM has also been seen to play a role in disease and cancer progression²⁶. Migration of cancer cells has been shown to be influenced by the ECM stiffness²⁷ in addition to the ECM structure and dimensionality^{28,29}. For brain tumors, such as the development of glioblastoma in a usually soft brain tissue environment, increased stiffness has been observed to influence tumor invasion, drug resistance, and disease recurrence³⁰. Stiffer tissue is also seen in breast tumor

environments, where elastic modulus can increase 10 fold, progressing the cancer through stiffness mediated signaling³¹. These changes in breast tissue ECM elasticity can lead to poorer treatment outcomes, increased cell migration, and proliferation³²⁻³⁴. These changes in cancer ECM stiffness are so common that monitoring for them, though palpation, for example, is one of the more used and easier ways to diagnose²⁶. Therefore, the development of 3D culture models that accurately replicate this ECM stiffening behaviour is essential to our understanding of disease progression and development of treatment.

This understanding of how a material's elastic properties influence cell and tissue behaviour has increasingly improved over the past two decades. However, more recently it is believed that not only the elasticity of the ECM is important but its plasticity⁷, that is the ability for the material to non-reversible deform under a sufficiently intense applied force³⁵. Inclusion and control of plasticity along with elasticity would allow for a more complete biomechanical picture when engineering 3D culture models. Plastic deformation of the cellular environment shows up in many aspects of cell and tissue behaviour. Buchmann et al. showed that branching of human mammary organoids caused plastic reorganization of the collagen hydrogel they were embedded in, leading to further branch outgrowth and more plastic deformation³⁶. This remodelling has been observed in a range of cell types, such as fibroblasts^{37,38}, breast tumors^{39,40}, artery smooth muscle⁴¹, and human umbilical vein endothelial cells⁴⁰, underlying the importance of considering the ECM reorganization ability in creating 3D models. Plastic remodeling, in conjunction with ECM porosity and degradability, mediates confinement of tissues in a matrix governing key cell functions such as cell growth, spreading, and migration, as well as proliferation, organoid formation, and matrix deposition (Figure 2)^{6,7,12,42-45}.

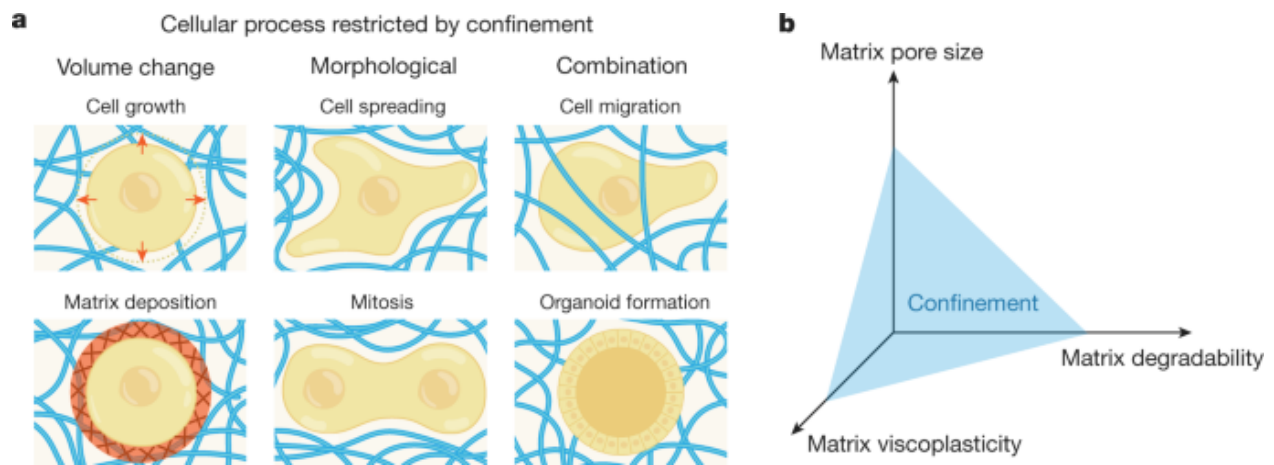


Figure 2: Cell functions dependent on hydrogel pores, degradability, and plasticity. a) Cell functions that are limited due to tissue culture materials lack of plastic or viscoplastic behaviour. b) Intersection of ECM degradability, pore size, and plasticity as factors for tissue confinement. Reprinted by permission from Springer Nature Customer Service Centre GmbH: Nature, Effects of extracellular matrix viscoelasticity on cellular behaviour. Chaudhuri et al., copyright 2020 ⁷.

Like ECM elasticity, it is also believed that ECM plasticity can play a role in disease progression and stem cell differentiation, but it is not as well studied and characterized. For example, we are beginning to understand how plastic remodeling of ECM is linked to invasiveness of breast cancer ⁴⁶, or how changes in lung ECM plasticity fits into the progression of fibrosis ⁴⁷. A recent study has looked to lay the groundwork for exploring the plasticity of Matrigel and collagen in regards to organogenesis ⁴⁸, however this is just the tip of the iceberg as more work needs to be completed to understand this complex mechanical property and its role in tissue fate and function. One of the largest barriers to understanding plasticity is the lack of suitable platforms allowing control over this property. While natural hydrogels like Matrigel exhibit these behaviours, they lack the tunability that would come with a synthetic hydrogel. As it stands, there is currently no synthetic hydrogel platform designed specifically for the study of ECM plasticity. This defines the need for a 3D culture platform that allows for the tuning of plasticity independently of its other material properties.

2.2 Defining and Classifying Hydrogels

Hydrogels are one of the most common biomaterials used in 3D tissue cultures, but selection of the proper gel requires knowledge of the ECM conditions being replicated and which hydrogel is able to accurately reproduce it. Gels can be categorized in a variety of ways, with the simplest

and most common being the source of the gel, either natural or synthetic ⁴⁹, or in some cases a composite hybrid of both. Naturally derived gels would include the likes of alginate, chitosan, and collagen-based hydrogels and even the mouse derived Matrigel ^{5,50-54}. Typically, a natural hydrogel is easy to source, relatively inexpensive, inherently biocompatible, and can have other attractive features such as innate biodegradability ⁵⁵. For instance, alginate is derived from brown algae, it is biocompatible and from a renewable source, allows for encapsulation of tissue during gelation, and can be selectively biodegraded ^{56,57}. However, natural hydrogels are not without their disadvantage. They are often mechanically weaker than their synthetic counterparts, can be poorly defined, and have a higher batch to batch variation in their chemical composition and physical properties, leading to poor reproducibility, which is often a problem when handling natural hydrogels such as Matrigel ⁵⁸⁻⁶⁰.

Synthetic hydrogels look to address some of the shortcomings seen with natural gels. This includes less variability in composition and material properties as well as higher mechanical strength ^{61,62}. Creation of a synthetic gel also allows for the selection of multiple different monomers to form copolymer gels with unique properties ⁶³. Poly(vinyl) alcohol, for example, can be used to form a gel suitable to study stiffer tissues such as cardiac muscle or bone tissue ^{64,65}. The much more complex poly(butyl methacrylate)-*b*-poly(methacrylic acid)-*b*-poly(butyl methacrylate) copolymer hydrogel allows for unique geometries and a controlled rate of drying and swelling ⁶⁶. One of the most commonly used synthetic gels in studying biomechanics is polyacrylamide (PAAm) due to its well characterized properties and established protocols ⁶⁷⁻⁶⁹, and while normally non-adhesive, it can be coated with collagen for cell culture ⁷⁰. The purely elastic PAAm hydrogel properties are reproducible, allow for a range of mechanical stiffnesses, are relatively low cost, and can be combined with other components or modified into copolymers for unique properties such as a PAAm-polyacrylic acid gels with silver nanoparticles for antimicrobial properties ^{63,71,72}. The disadvantages to synthetic hydrogels include their lack of bioactive properties, difficulty in cell recovery, and potential for harmful pre-gelation components or by-products that can be left in the hydrogel after gelation ^{73,74}.

Hybrid hydrogels aim to combine the advantageous properties of different natural and synthetic polymers into one gel, and can even allow for novel characteristics or unique structural

organization ^{75,76}. When engineering a hybrid hydrogel, synthetic components can allow for finer control of its material properties or allow for higher mechanical strength; natural components such as peptides and proteins can provide unique properties such as phase transitions or degradation ⁷⁵. An early example is the work completed by Wang et al. where the combination of a well-defined water-soluble synthetic polymer with a temperature responsive coiling protein allowed for the formation of a thermoresponsive volume changing hydrogel ⁷⁷. Other examples of hybrid gels include a collagen-poly(ethylene glycol) gel where the collagen can be selectively degraded, while the synthetic portion increases mechanical strength and stability ⁷⁸, gelatin methacryloyl-ferritin hydrogels where the ferritin protein allowed for better tuning of mechanical properties and controlled release of small chemical compounds ⁷⁹, or a hyaluronic acid gel reinforced with polycaprolactone that provided spatial cues for vasculogenesis ⁸⁰. The creation of different hybrid gels is potentially endless because of the various combinations of natural and synthetic gels, allowing for precise tailoring of hydrogels to specific biomedical applications ^{81,82}.

Classification of hydrogels is not just limited to their sources, but through a wide array of their properties, fabrication methods, responsiveness, or behaviour (Figure 3) ^{62,83}. Gels can be categorized by composition; homopolymer for gels of a single monomer type such as a PAAm gel ⁶⁹, copolymer or multipolymer for two or more types of monomers in a chain like a PAAm-polyacrylic acid gel ⁷¹, or the distinct interpenetrating networks where one polymer type is diffused into another as seen with the complex 'triple network' alginate-PAAm gel that is reinforced with dispersed graphene oxide sheets ⁸⁴. Another way to categorize hydrogels is their responsiveness to external stimuli. Either a conventional gel with no responsive behaviour or a smart hydrogel that could respond to various cues, which can be further sub classified into chemical, biochemical, or physical responsiveness. A poly(N-isopropylacrylamide) based hydrogels for example would respond to an increase in temperature by shrinking due to a change in polymer chain hydrophobicity and expulsion of water from its network ^{85,86}. Other examples include physical stimuli of pressure, light, or electromagnetic fields, chemical stimuli of pH changes or specific molecules such as sugars, and biological stimuli of antigens and enzymes ⁸⁷⁻⁹⁴. Additional classification categories of hydrogels include the type of crosslinking, be it physical

or chemical or if the links are cationic, anionic, or non-ionic; the gels degradability; or its physical characteristics like pore size, crystallinity, and physical shape and size^{59,62,83}. These classifications of hydrogels allow for an easy understanding of their properties and can be used for selection of the proper gel for the desired application.

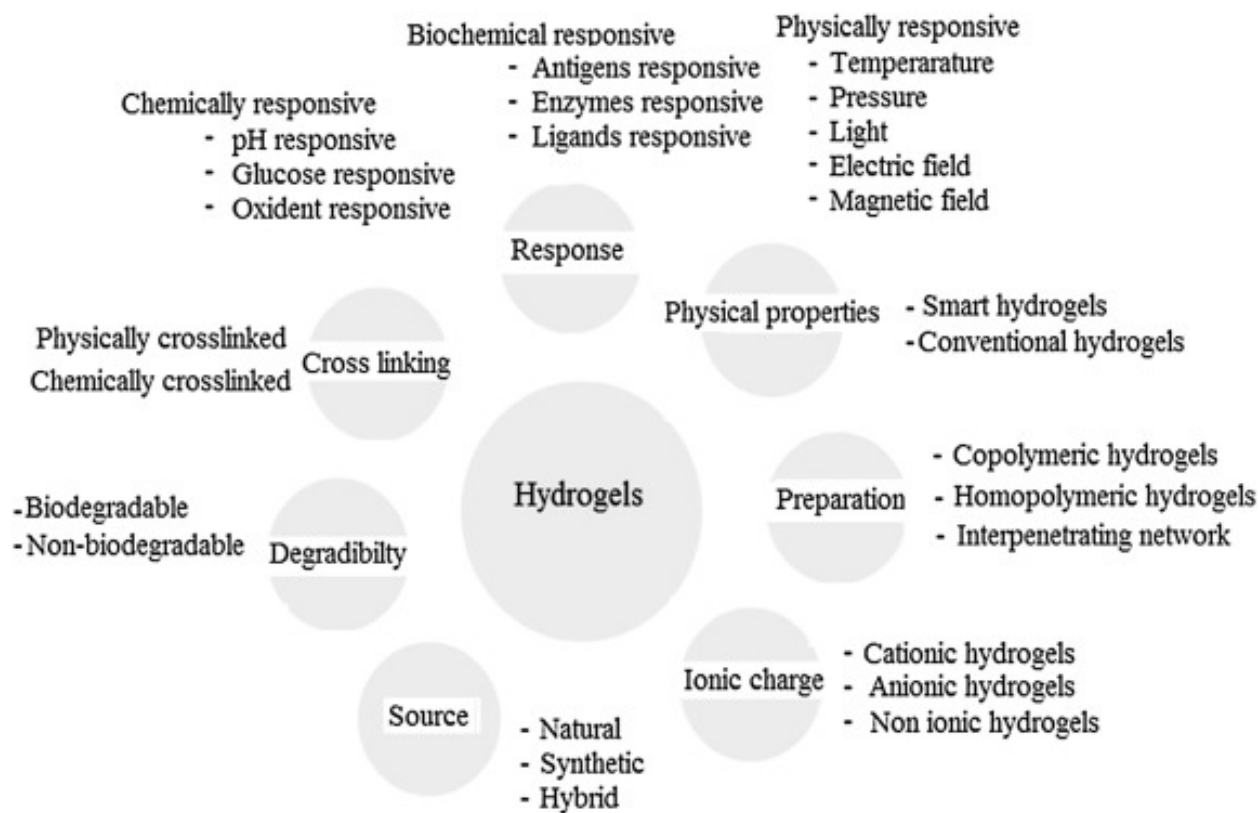


Figure 3: Hydrogel categorization. Categories of hydrogels based on their various chemical and physical properties, responsiveness, behaviour, sources, and crosslinking types. Reprinted from Materials Science and Engineering: C, 57, Ullah et al., Classification, processing and application of hydrogels: A review, 414-433, Copyright 2015, with permission from Elsevier⁸³.

2.3 Granular Hydrogels

A recently emerging subtype of hydrogel is the packed granular hydrogel, sometimes referred to as a packed microgels, microbead, or microparticle hydrogel. Here, hydrogels are created at the micron scale allowing for unique properties when packed together or incorporated into traditional bulk gels. Fabrication of these microgels can be done in a variety of ways, each with their own strength and drawbacks (Figure 4). Emulsion techniques require the use of an immiscible pre-gel in a secondary solution, such as formation of PAAm granules in a kerosene

bath undergoing vortexing ⁹⁵. This vortex emulsion method is straight forward and allows for large production of gels, requiring at minimum a vortex and an adequately sized vessel (Figure 4a) ⁹⁶. Recent work has even shown this method used to encapsulation of cells ⁹⁷. One of the largest drawbacks of this method is the high distribution of bead sizes, making it unsuitable for applications that require tight control over individual bead diameter ⁹⁸. A method that can be used if a narrow size distribution is required is the use of a two-phase microfluidic device (Figure 4b) ⁹⁹. Here, the oil phase is fed into the main microfluidic channel and the gel phase is added at a slower rate, allowing for individual granules to gel as it flows through the channel, with bead size being controlled through the microfluidic channel geometry and fluid flow rates ¹⁰⁰. Various geometries for this include a multi junction flow where the gel phase flows through a central channel and the oil phase is added through two side channels, a T-junction device where the oil runs along a main channel and the gel phase is added through one side channel, or coaxial channels where a smaller gel phase channel runs inside the oil phase channel before combining for droplet formation ¹⁰¹. Advantages of this technique could be the encapsulation of single cells within gels allowing for the study of individual cell behaviour, encapsulation of a specific molecule such as for analysis of a protein or DNA, or the creation of non-spherical particles such as a spiky hydrogel for drug delivery ¹⁰²⁻¹⁰⁵. The major drawback for microfluidic methods come in their slower production of microgels compared to that of other techniques, but can be improved through multiplexing of channels and advancement of device design ^{106,107}. Another drawback for both the two-phase vortex batch and microfluidic emulsion techniques is the required post-gelation separation and washing steps required to remove any harmful oils from the reaction ⁹⁶.

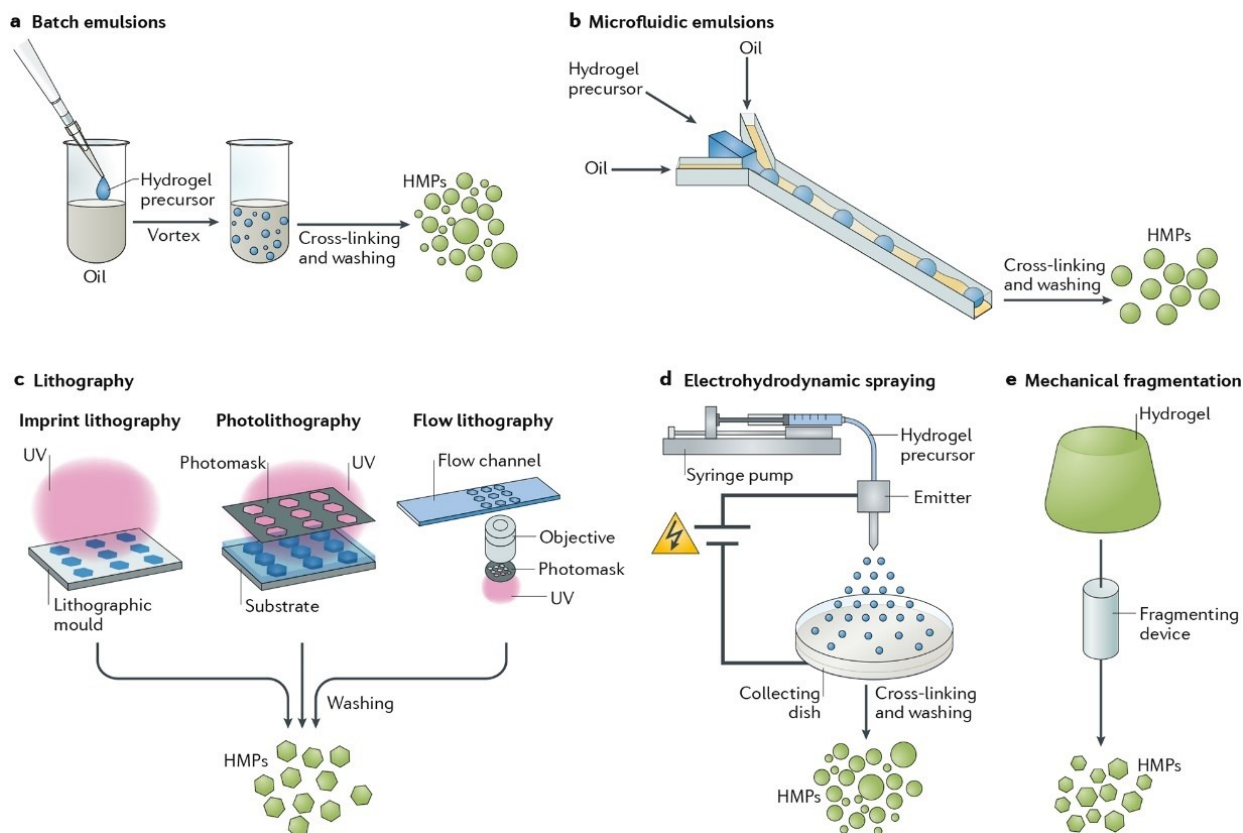


Figure 4: Granular hydrogel fabrication techniques. a) Batch emulsion of an immiscible gel solution in a second phase allowing for large batches of gels. b) Microfluidic multichannel devices for two phase fabrication for higher control of bead sizes. c) Lithography techniques for gelation of individual small particles through use of a template. d) Electro spraying of beads where an electric field is used to form beads. e) Mechanical fragmentation when a larger traditional bulk gel is broken into smaller micron sized particles. Reprinted by permission from Springer Nature Customer Service Centre GmbH: Nature, Nature Reviews Materials, Hydrogel microparticles for biomedical applications, Daly et al., copyright 2019⁹⁶.

Lithography has also been employed to fabricate microgels (Figure 4c). The use of a mask and different lithography techniques allows for unique and complex geometries and production of highly uniform microgel sizes, but at the expense of a much slower rate of production and limitation on size due to mask resolution^{108–110}. A less commonly used technique is electrohydrodynamic spraying (Figure 4d), where a voltage is applied to the gel ejection needle to form the microgel sphere which is then crosslinked in a collection bath, with size of the beads being dependent on ejection parameters such as voltage, needle gauge, and flow rate^{111,112}. This method allows for fabrication of large bead batches as well as the possibility of making non-spherical shapes¹¹³. However, electrohydrodynamic spraying requires a more complicated set up, while also having a higher size distribution, making it less favourable to other approaches¹¹⁴.

Finally, perhaps the simplest method of microgel fabrication would be mechanical fragmentation (Figure 4e). The use of microscale pore meshes, blending, or needle extrusion of a bulk gel is completed to physically break a conventional bulk gel into the microgels ^{115–117}. While this methods is simple and allows for fast production of granules, it produces them with little to no control over shape or size ^{96,117}.

Packed granular hydrogels have unique properties that can be utilized that are not seen in bulk hydrogels. Due to their granular nature, these types of gels can be shear thinning and self-healing ¹¹⁸. These behaviours allow for application as injectable scaffolds and in 3D printing, such as the work completed by Feig et al. on the injection of neural progenitor cells into rat brain tissue via conductive granular gels ¹¹⁹, the hyaluronic acid based granular gel developed by Muir et al. with improved mechanical and structural properties for 3D printing ¹²⁰, or the method of printing 3D alginate structures using a Carbopol microgel bath for a ‘printing-then-gelation’ approach developed by Jin et al. ¹²¹. Further, it's believed that injectable microgels will be a valuable tool in directing tissue repair and drug delivery ^{122,123}.

The inherent porosity between the packed granules is another appealing property (Figure 5). Pore size throughout the gel can dictate the transport of nutrients to encapsulated cells or aggregates, and even play a role in cell morphology, proliferation, spreading, and migration ^{124–126}. Granular gels can be interlinked, commonly seen in 3D printing techniques, to provide structure and stability after gelation (Figure 5), such as covalent ¹²⁷ or photoinitiated crosslinking between beads ¹²⁸. Microgels also allow for mixing of different gel types with unique functionalities to create heterogeneous packed gels, through either a uniform distribution of granules or a careful spatial arrangement such as layering of different gel types via 3D printing technologies ^{129,130}.

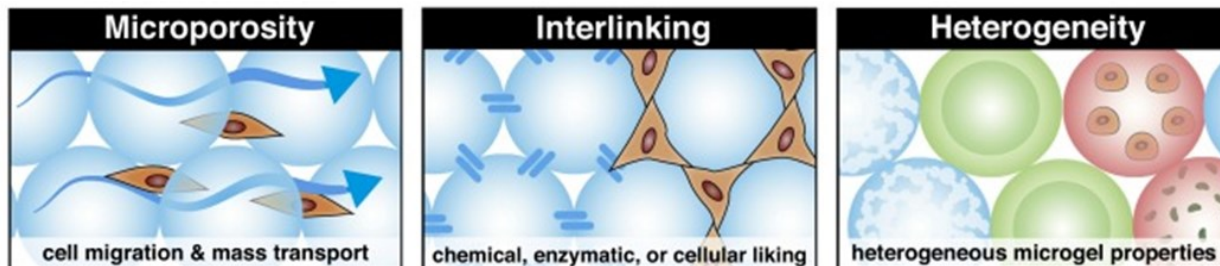


Figure 5: Inherently unique properties of granular hydrogels. left) Microporosity due to voids between beads providing space for cell migration and nutrient transport. mid) Methods of interlinking beads, providing structure and support to the bulk packed gel. right) Heterogeneous packed gels of different bead types providing unique functions or properties to the overall gel. Reprinted from *Current Opinion in Biotechnology*, 60, Riley et al., Granular hydrogels: emergent properties of jammed hydrogel microparticles and their applications in tissue repair and regeneration, 1-8, Copyright 2019, with permission from Elsevier ¹²⁹.

Understanding and characterizing packed granular gels is usually completed by measurement of their rheological properties and physical characteristics, as well as observation of cell response ¹¹⁸. For rheological properties, this includes mechanical moduli such as storage and loss modulus, yield point, shear thinning and self healing behaviours, which are dependent partly on the interlinking, or lack thereof, for the individual beads ^{118,131,132}. Packed gels can also be characterized by their bead size and overall size distribution, the porosity of the packed gel, the packing structure, and in some cases, the microscale roughness of the beads ^{133–135}. Perhaps the most important characterization of packed gels, in regard to tissue engineering, is cell and tissue response. This could include the behaviours of cell migration, proliferation, and spreading, stem cell differentiation, and organoid growth and invasion ^{136–141}.

2.4 Guest-Host Complexes

In recent years, supramolecular guest-host chemistry has been of increasing interest for their distinctive non-covalent interactions ¹⁴². Here, a host molecule such as cyclodextrin, urea, or cyclo-triphosphazines, partially or fully uptake a guest molecule, such as adamantane, phenylalanine, or aromatic amino acids, to form an inclusion complex with good stability (Figure 6) ^{143,144}. Because of this unique interaction, guest-host complexes have been increasingly studied for applications such as antimicrobial biomaterials, drug delivery systems, or even in sensors ^{145–147}. These dynamic bonds also allow for tuning of their interaction via external stimuli. For example, a pH responsive guest-host complex for drug delivery to lung metastasis ¹⁴⁸, a unique

magnesium based thermoresponsive host that captures and releases cyclodextrin as the guest ¹⁴⁹, or a guest-host material with switchable antibacterial to bioadhesive properties due to light exposure ¹⁵⁰. Guest-host interactions have also been developed that respond to enzymes, magnetic, and mechanical stimuli ^{151–154}.

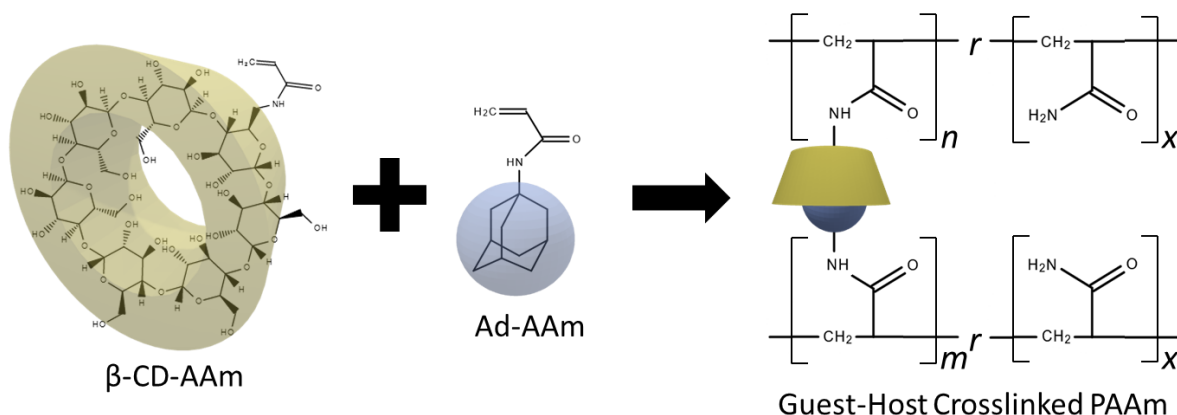


Figure 6: Formation of guest-host PAAm crosslinking. Interaction of beta-cyclodextrin-acrylamide (βCD-AAm) host molecule with adamantane-acrylamide (Ad-AAm) guest molecule for the crosslinking of polyacrylamide (PAAm) chains.

Specifically, how guest-host interactions respond to external stimulus is of great interest to the development of smart hydrogel systems. Incorporation of these complexes have been shown to bolster hydrogels mechanical properties, such as the α -cyclodextrin host dodecanoic acid/cellulose guest complex improving a PAAm hydrogels mechanical strength 6 fold ¹⁵⁵, or the addition of a β -cyclodextrin host adamantane guest crosslinker can create a highly elastic and reversible stretchable PAAm gel ¹⁵⁶. They can also be used to provide self healing behaviour to hydrogels, where these guest host interactions can be split apart but then rebind when brought back together, like the work completed by Ren et al. for a chitosan-based hydrogel sensor that displays this ability ¹⁵⁷, or the self-healing gelatin methacryloyl hydrogel developed by Wang et al. for use in 3D printing ECM scaffold ¹⁵⁸.

One specific property that these guest-host interactions are capable of is providing plastic deformation behaviour to an otherwise purely elastic material. As shown by Kakuta et al., the addition of β -cyclodextrin and adamantane as a crosslinker creates a highly elastic gel with reversible deformation (Figure 7a) ¹⁵⁶. However, they showed that at high enough strains the PAAm based hydrogel entered into a plastic region with non-reversible deformation (Figure 7b),

and further to a breaking point of the gel (Figure 7c) ¹⁵⁶. While this work begins to touch on plastic deformation in hydrogels, there is still a lack of research completed in exploring how this property plays a role in cell and tissue behaviour for both traditional bulk and granular packed hydrogels.

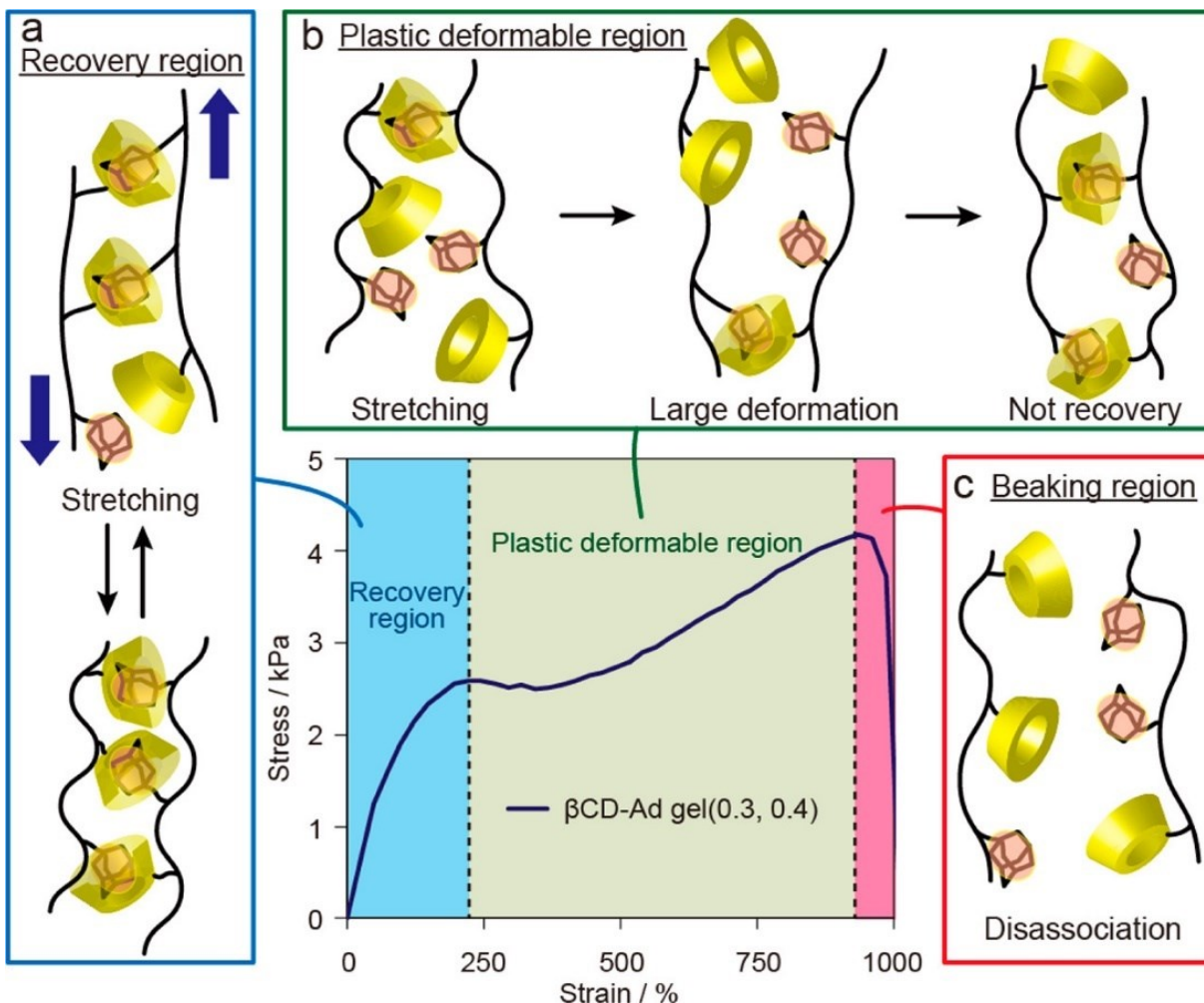


Figure 7: Stress-strain curve for a PAAm hydrogel with β CD and Ad crosslinking. Proposed mechanism for the guest-host crosslinked hydrogel gels behaviour in the a) elastic recovery region, b) plastic non-reversible deformation region, and c) after the breaking point. Reprinted with permission from Kakuta, T., Takashima, Y. & Harada, A. Highly Elastic Supramolecular Hydrogels Using Host–Guest Inclusion Complexes with Cyclodextrins. *Macromolecules* 46, 4575–4579 (2013). Copyright 2013 American Chemical Society ¹⁵⁶.

3 Approach

Currently, research into mechanical signaling of the ECM on cell and aggregate behaviour is largely focused on material elasticity. The plasticity of the ECM and its effects in 3D cultures is largely unknown. As it stands, there is no 3D culture platform specifically tailored to the study of plasticity, hindering our understanding of this mechanical property. This work set out to address this need by designing and tuning a plastically deformable hydrogel platform. PAAm was selected as the basis for its biocompatibility, well established formulations and protocols, and ability to alter the polymer chain through modification of the AAm monomer. β -cyclodextrin and adamantane were used as host and guest molecules to modify AAm monomers. Incorporation of these monomers into PAAm has been shown to provide plastic deformation behaviour. A granular hydrogel approach was selected as functionalization with the guest or host molecule would allow for interlinking between beads, such that bonds can break apart, beads can move past each other, and the interlinking reform. Utilizing the self-healing properties of the packed beads allows for a plastic deformation of the granular gel under mechanical force (Figure 8). Characterization of the granular packed gel was set about by rheological characterization of its shear elastic storage modulus and yield point into the plastic region. Finally, the platform was applied to an aggregate culture as a first proof of concept. Different levels of interlinking between beads as well as individual bead stiffness were explored for their influence on aggregate growth and invasion compared to a linearly elastic non-degradable hydrogel of varying stiffnesses.

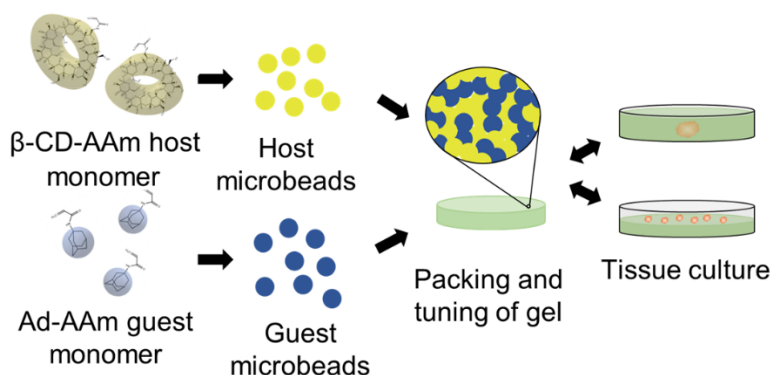


Figure 8: Granular packed hydrogel fabrication workflow. Simplified workflow of fabricating and applying the packed granular hydrogels. AAm monomers are functionalized with a guest or host molecule, microbeads are created and packed together to study their properties and the eventual application to cell and tissue cultures.

4 Materials and Methods

4.1 Bulk hydrogel fabrication

Bulk PAAm gels were created for use as described previously⁶⁹, with formulations as listed in table 1.

Table 1: PAAm gel formulations for 1000 μ L of gel. From ⁶⁹

Formulation (AAm%/Bis% (w/v))	3/0.05	3/0.1	7.5/0.05	12/2.5
40% Acrylamide (μL)	75	75	187.5	300
2% Bisacrylamide (μL)	24.5	53.5	118.0	120.5
PBS (μL)	799.0	770.0	684.0	478.0
TEMED (μL)	1.5	1.5	1.5	1.5
1% APS in PBS (μL)	100	100	100	100
Total	1000	1000	1000	1000

In brief, different weights per volume of acrylamide (AAm) (Bio-Rad) were combined with a bis-acrylamide (Bis) (Bio-Rad) crosslinker in phosphate buffered saline (PBS) (Sigma), along with tetramethylethylenediamine (TEMED) (Sigma) as a catalyst. A separate solution of ammonium persulfate (APS) (Bio-Rad) in PBS was created and added to the AAm pre-gel solution to initiate the reaction. The mixture was vortexed briefly, pipetted onto an 18 mm cover slip (Fisher), covered with an additional coverslip, and allowed to gel at room temperature for 45 minutes before being transferred directly into a 6 well plate (Fisher), covered in PBS, and left on a shaker plate for 1 hour to aid in coverslip removal and as a first wash. Coverslips were removed, PBS was replaced, and left for another 30 minutes before repeating the PBS wash one more time. Once the washing steps were completed, samples were allowed to swell overnight in PBS at 4 °C and stored sealed with paraffin until use.

4.2 Preparation of β -cyclodextrin and adamantane acrylamides and dyes

β CD-AAm was synthesized based on the protocol of Kakuta et al.¹⁵⁶. In an ice bath, 6-Amino- β CD was dissolved in 0.1 M solution of sodium bicarbonate (Sigma) and pH adjusted to 10 using a sodium hydroxide solution (Sigma). Acryloyl chloride (Sigma) was added dropwise and left to react for 8 hours. The solution was then evaporated to 40% of the total volume and precipitated in acetone. The precipitate was collected and freeze dried. The product was purified with a HP-20 polystyrene gel (Sigma) using a gradient of water/methanol to yield β CD-AAm. Functionalization was confirmed using nuclear magnetic resonance.

Ad-AAm was also synthesized based on the protocol of Kakuta et al.¹⁵⁶. In an ice bath, adamantylamine and triethylamine (Sigma) were dissolved in tetrahydrofuran (Sigma). Acryloyl chloride was added dropwise and left to react overnight. The precipitate was removed by filtration, and the supernatant was freeze dried overnight. Using silica gel column chromatography, the crude product was eluted with hexane/ethyl acetate to yield pure Ad-AAm. Functionalization was confirmed using nuclear magnetic resonance.

To form the β CD and Ad fluorescein dyes, 6-Amino- β CD or Adamantylamine was dissolved in PBS and NHS-Fluorescein (Fisher) was added in 1:1.25 ratio. The mixture was allowed to react to completion overnight and used as is.

4.3 Granular hydrogel fabrication and assembly

AAM and APS solutions were created as described above in separate glass tubes (VWR) equipped with a rubber septum stopper. For host granular hydrogels, β CD-AAm was added directly into the AAm pre-gel solution. A third glass tube, with a stir bar, was prepared with a 6% (v/v) polyglycerol polyricinoleate (PGPR) (Palsgaard) in kerosene (Sigma) solution, at a volume of 3 ml kerosene solution to 1 ml of prepared pre-gel solutions (AAM and APS combined volumes). For guest granular hydrogels, Ad-AAm was included in the kerosene solution. The three glass tubes were then closed, and a septum penetration needle (Fisher) attached to a nitrogen gas supply was placed through the rubber stopper and into the depth of the liquid. An additional needle was used as a vent and the tubes were purged with nitrogen for 20 minutes.

After nitrogen purging, the APS solution was taken up into a syringe through the septum needle and added to the AAm pre-gel. Working quickly, the mixture was vortexed briefly, taken up by a second syringe and septum needle, and injected into the kerosene solution. The two-phase liquid emulsion was then vortexed on a Vortex Genie 2 (Scientific Industries) for a set time according to the desired bead size and left on a stir plate for a total of 15 minutes at 1000 RPM.

After gelation, fresh kerosene was added to the two-phase emulsion, vortexed lightly, and allowed to settle via gravity. The top kerosene phase was removed, and the kerosene wash repeated for a minimum of 3 times, until there was no noticeable change in the translucency of the supernatant. The top kerosene phase was then completely removed and the remaining microgels transferred in 0.5 ml amounts to 1.5 ml Eppendorf tubes (Sarstedt) and topped up with PBS. Tubes were centrifuged at 14,000 rpm (21,000 RCF) for 2 minutes. Top layers of kerosene and PBS were removed and replaced with fresh PBS. The packed gel pellet was resuspended via pipette, centrifuged back down, and the process repeated multiple times. The bead suspension was transferred to new Eppendorf tubes after 2-3 washes. Washes were stopped once the beads were cleaned of the white surfactant residue. A sample of beads was examined under a microscope to confirm cleanliness and proper gelation. Microgels were gathered in a single 15 mL tube, suspended in fresh PBS, and left overnight to swell at 4 °C.

4.4 Imaging and analysis of hydrogels

Size measurements of microgels were completed by inclusion of 0.2 μm FluoSpheres carboxylate-modified red beads (Life Technologies) into the AAm pre-gel solution before microgel fabrication allowing for easier recognition during image analysis. Images were taken with a EVOS M7000 Cell Imaging System (Fisher), and the bead size was analyzed in FIJI ¹⁵⁹.

Fluorescein conjugated Ad and βCD used to allow for visualization and fluorescent intensity quantification of Ad and βCD functionalization in microgels. Fluorescein-Ad dye was added to βCD functionalized microgels, and fluorescein- βCD dye was added to Ad functionalized microgels at 5 $\mu\text{L}/\text{ml}$ of bead suspension. Samples were washed 3 times in PBS before plating and imaging with an Olympus IX73 Microscope. Fluorescent intensity was measured using FIJI ¹⁵⁹.

Visualization of Ad and β CD microgel interactions was completed by including 1 μ L of fluorescein o-methacrylate (100 mg/mL in DMSO) (Sigald) per 1 ml of Ad AAm pre-gel solution, and 1 μ L of 0.2 μ m FluoSpheres beads per 1 ml of β CD AAm pre-gel solution before microgel fabrication. Imaging of Ad and β CD bead and packed gels was completed using the EVOS M7000 system and analysis done using FIJI¹⁵⁹.

4.5 Micromanipulation of microgels

Fine control and manipulation of the microgels was completed using a TRIO™ MP-245 Micromanipulator System (Sutter Instrument) equipped with micropipettes fabricated on a Flaming/Brown Micropipette Puller Model P-97 (Sutter Instrument). A suspension of Ad microgels in PBS was placed in a well plate. Suction was applied to individual Ad microgels through the use of a syringe attached to the micropipette. The Ad microgels were contacted with a stiff bulk PAAm hydrogel, 12/2.5 (AAm%/Bis% (w/v)) functionalized with 24 mg/ml β CD, placed within the same well plate, and gently shaken to form a guest-host bond between beads and the bulk gel. Microgels were then grabbed with a micropipette using the micromanipulator and moved away to see stretching of the Ad microgels at the point of the guest-host bonds breaking. The Ad gel is then moved back to the surface of the β CD gel at the same point of contact and repeated until the manipulator lost suction on the Ad bead.

4.6 Rheological characterization of hydrogels

Mechanical characterization of bulk and granular packed hydrogels was completed using an Anton Paar MCR 302 Modular Compact Rheometer equipped with an 8 mm parallel plate geometry. Parallel plate geometry was selected as bulk hydrogels must be allowed to swell unconstrained overnight in PBS after gelation and subsequently would not conform to a cone and plate set-up without mechanically preloading the gel as material is pushed out from the center, or in a worse case causing the gel to break. As well, loading the granular gels required an adequately large gap size that is at least 10 times larger than the particle size, which is not possible in a cone and plate set up¹¹⁸. All samples were tested on the stage heated to 37°C. Bulk PAAm hydrogels were allowed to swell fully in PBS before placing them on the rheometer stage. The geometry was then lowered until a normal force between 0.04 and 0.10 N was measured.

The samples were then trimmed to the geometry for testing. Granular packed bead hydrogels were formed by combining equal volumes of Ad and β CD microgels. 500 μ L of Ad bead suspension at 100 μ L beads/ml PBS is added to 500 μ L of β CD bead suspension of the same concentration, gently pipetted to mix and centrifuged at 21,000 RCF for 2 minutes to form the bulk gel. Gels were transferred to the rheometer stage and the geometry lowered until the gel filled the sample space. Samples were then trimmed to the geometry size for testing. All samples were subject to an amplitude sweep from 0.01 to 1000% shear strain. Shear stress, storage modulus (G'), and loss modulus (G'') were measured and reported. Elastic modulus was determined from the linear region of G' reading and yield point was determined at a drop of 5% from the elastic modulus.

4.7 Cell and aggregate culture

Microgels for cell culture were created using a pre-gel solution that was sterilized through 0.22 μ m nylon syringe filters (Fisher). Fabricated microgels were resuspended in PBS with 1% (v/v) antibiotic-antimycotic (anti-anti) (Fisher) and left to sterilize under UV light at 36 W overnight. Microgels were then handled under sterile conditions in a biological safety cabinet (BSC). Microgels were centrifuge and the supernatant removed to prepare them for use.

The breast cancer cell lines MCF7s and T47Ds (ATCC), were used to study microgels cytocompatibility and in culture tests, respectively. Cells were cultured in Dulbecco's Modified Eagle's Medium (DMEM) high glucose (Fisher) supplemented with 10% (v/v) fetal bovine serum (FBS) (Fisher) and 1% (v/v) anti-anti at 37°C, 5% CO₂. Culture media was changed every two days. These cells were cultured in T-25 vented cap cell culture flasks (VWR). When the cells reached approximately 80% confluency, trypsin-EDTA (0.25% v/v) (Fisher) was used to detach cells. Cells were resuspended and plated in complete growth medium to the desired cell concentration or used in experiments.

To study the cytocompatibility of the fabricated microgels, 5 μ L of Ad or β CD microgels were plated in a 96 well plate (Fisher) with 200 μ L of complete growth medium. The plate was centrifuged at 200 RCF for 2 minutes. MCF7 cells were seeded at 1×10^4 cells per well for 4 wells total on day 0. Media was changed on day 2 and brightfield images collected on days 1 and 3 using the EVOS M7000 system. Cells were live/dead stained on day 3 with calcein AM (Life

Technologies), ethidium homodimer-1 (EthD-1) (Life Technologies), and Hoechst 33342 (Sigma). Calcein AM was added at a concentration of 2 μM for staining of live cells. EthD-1 was added at a concentration of 4 μM for staining of dead cells. Hoechst 33342 was added as a live nuclear label at a concentration of 2 $\mu\text{L/ml}$. Cell cultures were left to incubate at 37°C for 30 minutes before imaging. The number of live and dead cells were quantified using FIJI ¹⁵⁹. A parallel control culture was conducted following the same procedure but without the addition of microgels.

T47D aggregates were formed by seeding cells in arrays of 500 μm non-adhesive PAAm microwells. Wells were created as described previously for bulk PAAm gels on 3D printed moulds. Gels were created using a 12/2.5 (AAm%/Bis% (w/v)) formulation to create a very stiff PAAm microwell. Pre-gel solutions were filtered as previously described, and after gelation, placed in 12 well plates (Fisher), soaked in anti-anti and exposed to UV light for sterilization. T47D cells were prepared by suspended at 10×10^6 cells/mL media. 200 μL of cell suspension was pipetted to the microwell array surface and cells were allowed to settle into the wells for 5 minutes before excess media was aspirated. Seeded wells were supplemented with complete media, incubated at 37°C and 5% CO_2 , and allowed to self assemble into spheroids for 3 days before use.

Aggregates were embedded in both granular guest-host gels and a TrueGel3D Hydrogel kit (Sigma) as a linearly elastic, non-plastically deformable, and non-degradable control. Granular gels were prepared by first suspending Ad and βCD bead separately in media at 100 μL beads/ml. 50 μL of each suspension was added to a well of a 96 well plate, gently pipetted to mix and centrifuged using Sorvall Legend RT+ centrifuge (Fisher) equipped with a well plate attachment at 100 RCF for 2 minutes. T47D aggregates were transferred from the PAAm microwells to the guest-host bead bed using a cut tip pipette, at 2 to 6 aggregates per well, and centrifuged at 75 RCF for 2 minutes. 100 μL of Ad and 100 μL of βCD suspensions were added and centrifuged at 75 RCF for 2 minutes to encapsulate the aggregate. TrueGel9 TrueGel3D hydrogels were prepared according to the manufacturer's instructions. Briefly, the TrueGel3D buffer 10 \times concentrated, SLO-PVA, and water were mixed in a well of a 96 well plate before adding 2 to 6 aggregates per well. The polyethylene glycol (PEG) non-cell-degradable crosslinker was added to initiate gelation and was left to incubate for 1 hour at 37°C. Complete media was added to cover

the gel and left for an additional hour before being replaced with fresh media. Samples were monitored and imaged over 6 days. The size of the aggregates were measured using FIJI ¹⁵⁹.

4.8 Quantification of aggregate invasion

Invasion of the aggregates was characterized by measurement of an aggregate's circularity over time. Measurements of the aggregates were completed in FIJI ¹⁵⁹ with circularity defined as follows.

$$Circularity = \frac{Perimeter^2}{4\pi * Area}$$

This ratio allows for a normalized measure of the aggregate shape, where a value of 1 indicates a circular area and values above 1 indicates a deviation from a circular area. In this case, a significant deviation of the day-to-day circularity indicates invasion of the aggregate into the surrounding hydrogel as it shows tissue growth in one direction, away from the aggregate body, not associated with overall growth.

4.9 Creation of figures and statistical analysis of aggregate growth

Figures were created and analysis of the aggregates to compare growth on day 6 were completed in GraphPad Prism 9.1.2 for Windows, GraphPad Software, San Diego, California USA, www.graphpad.com.

Normality of the growth rate data sets was determined using a Shapiro-Wilk test. Equivalence of variance was assessed using a Brown-Forsythe test. As the data was determined to be normally distributed and the standard deviations were not statistically different, an Ordinary one-way ANOVA was completed followed by a Tukey's multiple comparison test.

Normality of aggregate invasion data sets was determined using a Shapiro-Wilk test. Sphericity was not assumed, and a Geisser-Greenhouse correction applied. Conditions were found to pass normality and a repeated measures one-way ANOVA was completed followed by a Tukey's multiple comparison test. Conditions that did not pass normality were assessed using a Friedman test followed by a Dunn's multiple comparison test. As the TrueGels are non-degradable and non-plastically deformable, a high level of confidence ($P < 0.001$) was selected to remove any differences due to the natural growth of the aggregate and any corresponding spread of the data.

The same level of confidence was applied to the packed bead invasions to look for deviation as a signal that invasion had occurred.

5 Results

5.1 Fabrication of guest and host functionalized PAAm microgels

PAAm microgels were fabricated using the vortex emulsion method. Sets of beads were made to study the effect of microgel size, microgel stiffness, and the amount of β CD-AAm and Ad-AAm included in the pre-gel setups on the mechanical properties of a packed granular hydrogel. Sets of PAAm microgels labeled with 0.2 μm FluoSpheres beads were created with an AAm/Bis ratio of 3/0.1 (w/v%), without either β CD or Ad, and with vortex times of 5, 30, and 120 seconds. Increasing the vortex time led to smaller overall microgel sizes and a narrower distribution of microgels (Figure 9a). Two separate microgels batches with an AAm/Bis ratio of 3/0.1 (w/v%) at 120 seconds vortex time were created for a β CD concentration of 24 mg/ml and an Ad concentration of 4 mg/ml to observe if the addition of the host or guest molecule influences the size of the fabricated microgels. Similar bead sizes and size distributions were seen in both the β CD and Ad functionalized microgels when compared to the unfunctionalized microgels of the same AAm/Bis ratio and vortex time (Figure 9b).

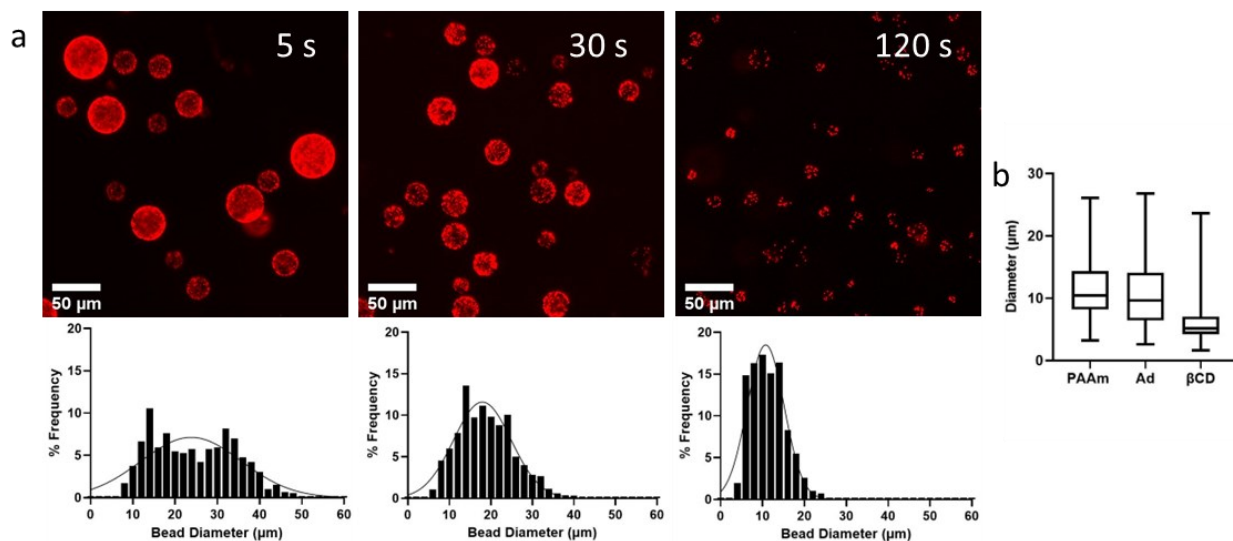


Figure 9: Granule hydrogel size as a function of vortex time. a) Distribution of bead sizes for emulsion vortex times of 5 seconds (left), 30 seconds (middle) and 120 seconds (right). b) Comparison of bead sizes for unfunctionalized PAAm, Ad functionalized PAAm, and β CD functionalized PAAm microbeads of a 120 second vortex time.

Microgels were fabricated with different amounts of guest or host molecules included into the pre-gel set ups. An initial concentration curve was created by adding fluorescein labeled guest or host molecules to samples of microgels to determine if there was a maximum or minimum threshold in the concentration of Ad or β CD functionalization to the PAAm microgels (Supplementary Figure 21). A plateau of maximum concentration was seen between 2 and 4 mg/ml for Ad, and only a slight decrease was seen between 12 and 24 mg/ml for β CD. A second set of beads were fabricated for Ad at 0.4, 0.8, 1.33, and 4 mg/ml, taking in mind the maximum concentration plateau. A second set of β CD beads were also fabricated at 2.4, 4.8, 10, and 24 mg/ml. Fluorescein dyes conjugated with either Ad or β CD were added to the β CD or Ad functionalized beads, respectively. The dyes were also added to unfunctionalized PAAm bead controls. A decrease in the fluorescence intensity was seen for both the Ad and β CD functionalized beads with decreasing Ad and β CD concentrations (Figure 10).

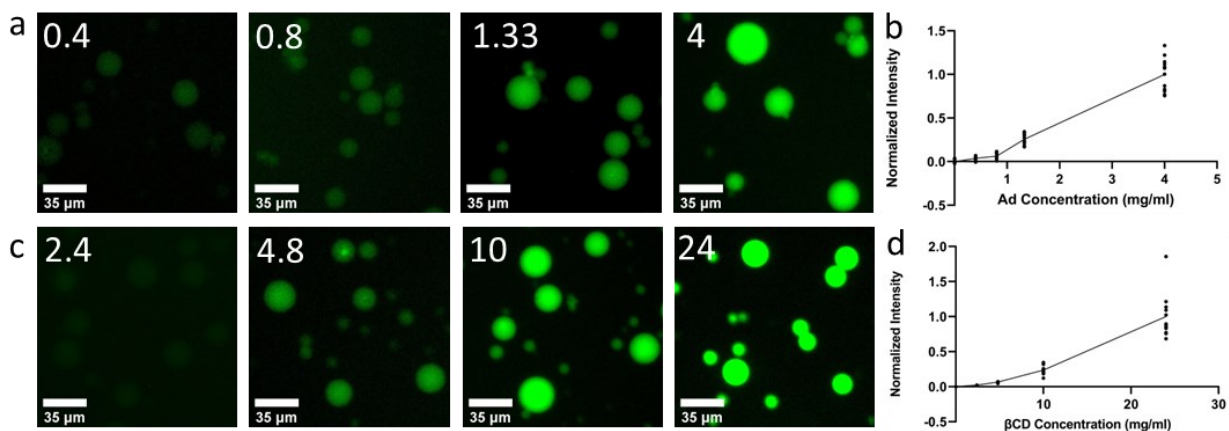


Figure 10: Granule guest and host functionalization. a) Fluorescent images of Ad functionalized beads for 0.4, 0.8, 1.33, and 4.0 mg/ml of Ad with a β CD-fluorescein dye. b) Normalized intensity of Ad functionalized beads. c) Fluorescent images of β CD functionalized beads for 2.4, 4.8, 10, and 24.0 mg/ml of β CD with an Ad-fluorescein dye. d) Normalized intensity of β CD functionalized beads.

Bulk PAAm gels were fabricated with different AAm%/Bis% ratios and tested using shear rheometry to confirm differences in the formulation's elastic properties. Bulk gels of 3/0.05, 3/0.1, and 7.5/0.05 (AAm%/Bis% (w/v)) were created. The three different formulations showed distinctly different storage moduli at 50 Pa, 335 Pa, and 2270 Pa for 3/0.05, 3/0.1, and 7.5/0.05 respectively (Figure 11).

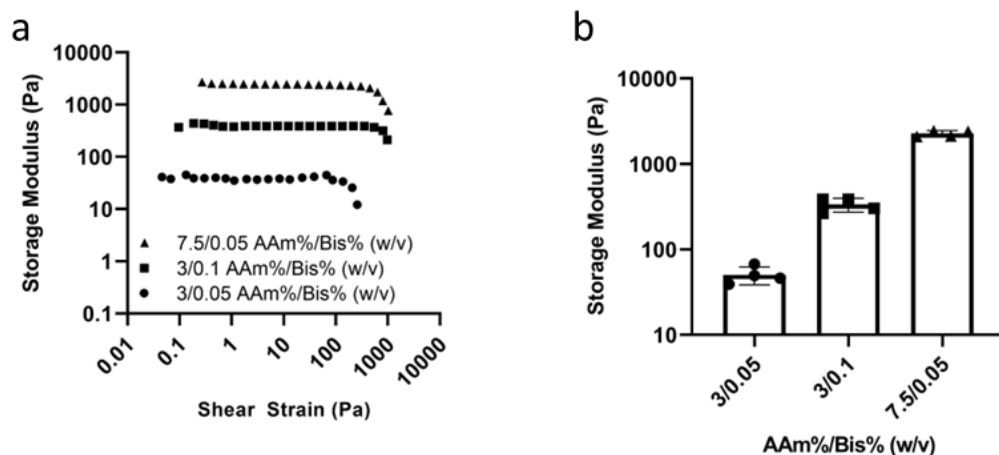


Figure 11: PAAm formulation storage modulus. Comparison of a) shear rheology amplitude sweep and b) measured storage moduli for different PAAm formulations.

5.2 Confirmation of guest and host interactions

Batches of Ad functionalized, β CD functionalized, and unfunctionalized PAAm beads were combined together to confirm packed gel formation and that formation is due to Ad- β CD interactions and not from other effects. Beads were mixed in equal parts for PAAm and β CD, PAAm and Ad, and β CD and Ad. Formation of a packed bulk gel was only seen with the Ad and β CD mixture, whereas the other combinations remained as a bead slurry (Figure 12).

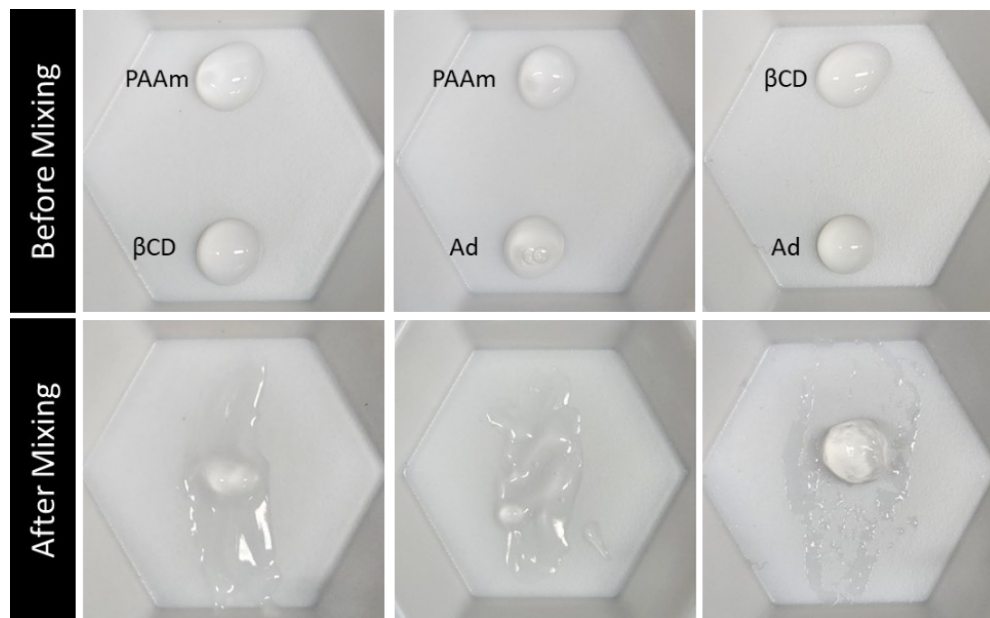


Figure 12: Mixing interactions of functionalized and unfunctionalized PAAm beads. Slurries of unfunctionalized PAAm beads mixed with β CD-PAAm beads (left) and Ad-PAAm beads (middle) staying as slurries, and β CD-PAAm beads mixing with Ad-PAAm beads to form a solid gel (right).

Ad and β CD beads were fabricated with fluorescein or 0.2 FluoSpheres beads respectively for both the 3/0.1 and 7.5/0.05 AAm/Bis (w/v%) formulations. Diluted samples of Ad and β CD beads were imaged to observe the guest-host interactions and microgel behaviour at the micron or bead-to-bead level. The softer 3/0.1 (335 Pa storage modulus) showed more deformation and increased areas of interaction between Ad and β CD bead types when compared to the stiffer 7.5/0.05 (2270 Pa) beads (Figure 13). The 7.5/0.05 beads maintained their spherical structure with less area of interaction between the Ad and β CD beads (Figure 13a). The deformation was not observed for beads of the same type (Ad to Ad or β CD to β CD) clumping together. Guest-host interactions between the beads were further observed using a micromanipulator set up, where interactions between unfunctionalized PAAm beads and interactions between guest and host functionalized beads were studied. All beads were fabricated at 3/0.1 AAm/Bis (w/v%), and functionalized beads were made with 4 mg/ml Ad or 24 mg/ml β CD. When contacted together, no signs of binding were observed for the unfunctionalized beads (Figure 13b), while binding between guest and host beads required little contact to occur and created strong interlinking as shown by the high degree of stretching without breaking of the bonds (Figure 13c).

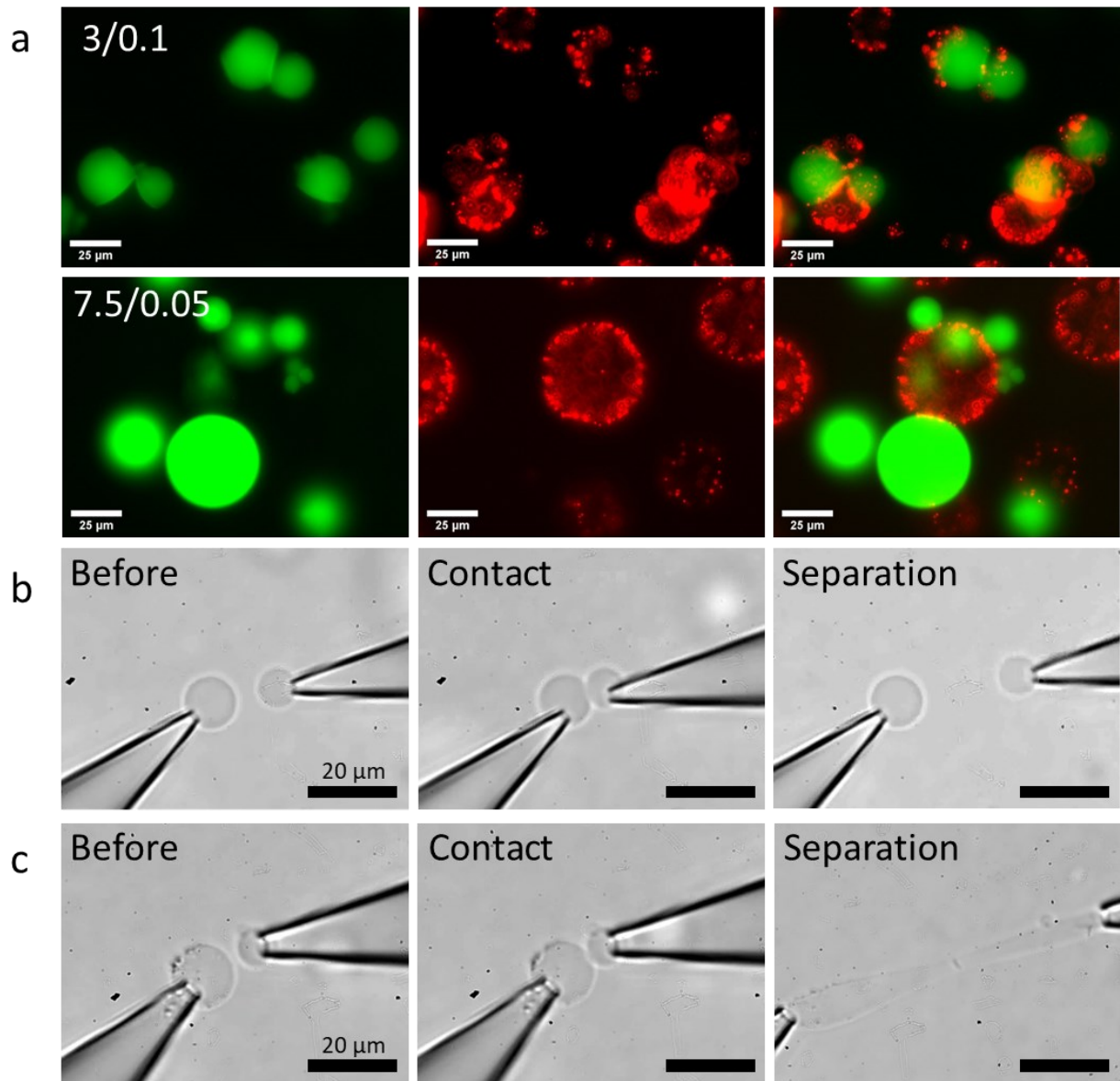


Figure 13: Soft and stiff guest and host granule interactions. a) Comparison of soft (top) and stiff (bottom) PAAm formulations interlinking, squishing together, and deforming due to guest-host interactions. Ad functionalized beads in green and β CD functionalized beads in red. b) Contact and separation of unfunctionalized PAAm hydrogels. c) Contact, binding together, and attempted separation of guest and host functionalized PAAm hydrogels.

To ensure uniform properties across a packed granular gel, mixing by hand and mixing via vortexing and centrifugation were compared. Equal parts Ad and β CD beads functionalized with fluorescein or 0.2 μ m FluoSpheres beads respectively were mixed with the end of a pipette tip. The resulting packed gel was then imaged for the two types of beads and normalized intensity compared. Imaging was repeated for gels mixed together in a diluted suspension, vortexed, and

centrifuged into a packed gel. Beads were less evenly distributed when mixed by hand, as normalized intensity readings showed pockets of lower fluorescence for both types of beads (Figure 14). Mixing via vortex provided a more uniform bead distribution and better mixing of the two bead types, which would lead to more uniform material properties throughout the packed gel (Figure 14).

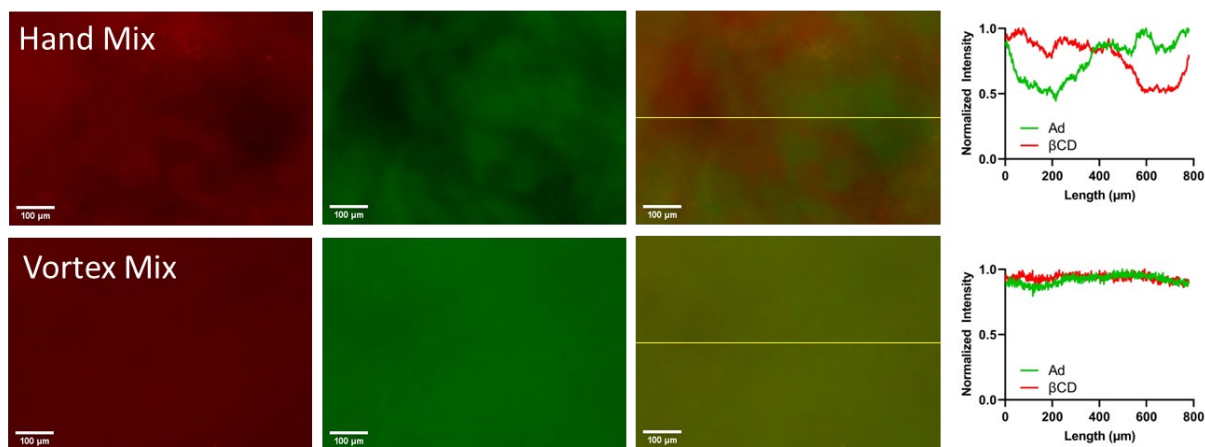


Figure 14: Effect of mixing methods on packed gels. Fluorescent images of mixed Ad (green) and β CD (red) functionalized PAAm granules. Distribution of beads for mixing by hand (top) and via vortexing and centrifuge (bottom), along with normalized intensity readings.

5.3 Repeated adhesion of Ad beads to β CD bulk gels

Ad functionalized beads were fabricated at 3/0.1 AAm%/Bis% (w/v), 1.33 mg/ml Ad, and vortex time of 5 seconds for larger beads that will provide a lower amount guest-host bonding. To demonstrate repeated binding of guest-host complexes, a dilution of beads were added to a stiff β CD functionalized PAAm block and allowed to bind to the surface then repeatedly removed and reattached. Detachment of the beads from the PAAm block occurred when moving directly away from the surface. For all trials completed, stretching at the point of detachment was measured along the semi-major axis and normalized to the unstretched bead diameter. Normalized detachment length followed a linear trend (Figure 15) with variations in stretched semi-major axis due to instability in micromanipulator speed and control of manipulator by hand. In all trials, the detachment attempts ended due to loss of suction from the micromanipulators on the Ad microgel and the bead adhering to the stiff bulk gel surface.

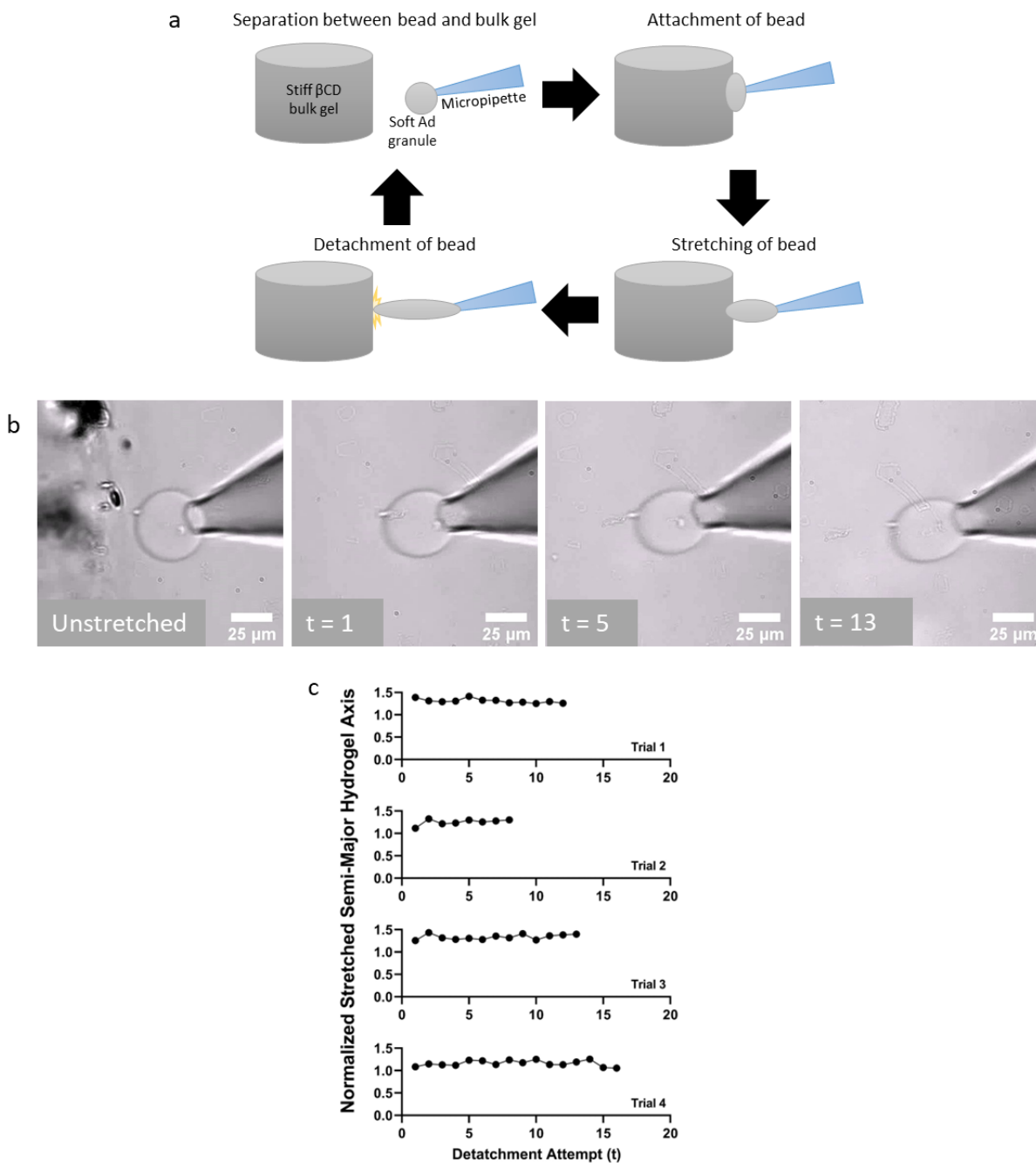


Figure 15: Repeatability of guest-host complex formation. Repeated adhesion and detachment of Ad functionalized PAAm granules on stiff β CD bulk gels. a) Schematic of the bead detachment and reattachment trials: Initial separation of bead from the bulk gel, attachment of the bead to the gel, movement away and stretching of the bead from the bulk gel, and detachment of the bead. b) Detachment images corresponding with trial 3, granule shown unstretched and at point of detachment 1, 5, and 13. c) Normalized length of the semi-major stretched axis with detachment attempts for four bead detachment trials.

5.4 Mechanical properties of packed granular hydrogels

Sets of packed guest-host granular hydrogels were created to measure their elastic and plastic properties. Shear rheometry was completed to quantify the packed gels storage modulus, a measure of the material's elasticity, as well as its yield point, a measure of when a material enters the plasticly deformable region. Packed gels were created for varying bead sizes, varying bead stiffnesses, and the concentration of Ad and β CD included in their respective beads. Equal amounts of the Ad and β CD beads were used in packing together the bulk gels.

To observe the effect of bead size on mechanical properties, packed gels were fabricated with vortex emulsion times of 5 s, 30 s, and 120 s, where the longer vortex time leads to smaller bead sizes. All beads were fabricated for 3/0.1 AAm%/Bis% (w/v), and 4 mg/ml of Ad or 24 mg/ml β CD. No observable difference was noticed in the storage modulus, while the yield stress decreased with decreased bead sizes (Figure 16a). However, the yield strain was comparable for all three conditions.

The three bead formulations, 3/0.05, 3/0.1, and 7.5/0.05 (AAm%/Bis% (w/v)), were tested to observe how individual bead stiffness plays a role in the bulk packed gel properties. Beads were fabricated at 120 s vortex time, and 4 mg/ml of Ad or 24 mg/ml β CD. An increase in bulk stiffness was seen with increasing individual bead stiffness. For the 3/0.05 formulation a storage modulus of 75 Pa was measured, 204 Pa for 3/0.1 formulation, and a value of 962 Pa for the 7.5/0.05 beads (Figure 16b). A similar trend was seen with the measured yield stress, where increasing bead stiffness led to a higher yield stress for the packed gels. Yield strain was observed to decrease slightly with increasing stiffness.

Four sets of beads were used to measure how decreasing amounts of Ad influences the packed gel mechanical properties. Concentrations of 4, 1.33, 0.8, and 0.4 mg/ml were tested. All beads were fabricated at 120 s vortex time, 3/0.1 AAm%/Bis% (w/v) and packed with β CD beads of a 24 mg/ml concentration. Overall bulk gel stiffness decreases as Ad concentration decreased, while yield stress decreases below an Ad concentration of 1.33 mg/ml (Figure 16c). Yield strain was observed to be similar across Ad concentration.

Similarly, four sets of beads were used to study decreasing β CD concentration in the packed gels. Concentrations of 24, 10, 4.8, and 2.4 mg/ml were tested. All beads were fabricated at a vortex time of 120 s, 3/0.1 AAm%/Bis% (w/v) and packed with Ad beads of a 4 mg/ml concentration. Overall bulk gel stiffness decreases as β CD concentration decreases, and a similar trend was observed for the yield stress with respect to the β CD concentration (Figure 16d). Yield strains were observed to be similar across β CD concentrations.

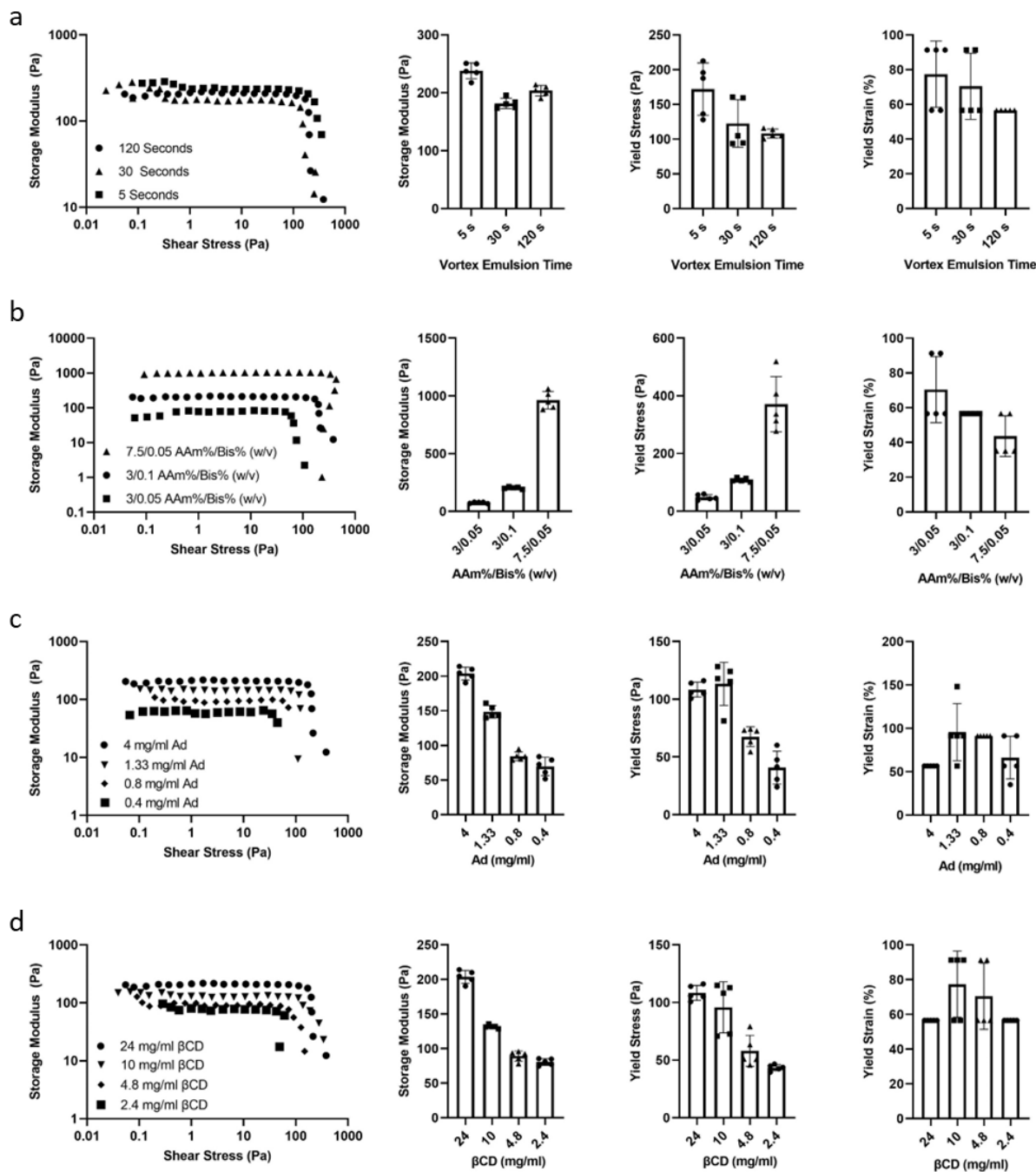


Figure 16: Rheological characterization of granular packed gels. Packed granular guest-host gels were fabricated and characterized for varying a) granule size presented as vortex emulsion times, b) granule stiffness presented as their AAm/Bis pre-gel concentrations, c) guest Ad concentration in the emulsion kerosene phase, and d) host β CD concentration in the pre-gel. From L to R, comparative amplitude sweeps of gels, storage modulus, yield stress, and yield strain are presented.

5.5 Plastically tunable granular hydrogels as an aggregate culture platform.

Guest and host granular hydrogels were assessed for their cytotoxicity with respect to the chosen model MCF7 breast cancer cell line. Ad and β CD beads were separately plated and MCF7 cells seeded on top and left for 3 days in culture, along with a control with no beads. Proliferation and spreading of cells was observed from day 1 to day 3 (Figure 17a). Comparably high cell viability was seen on day 3 for Ad and β CD cultures as well as in the control (Figure 17b).

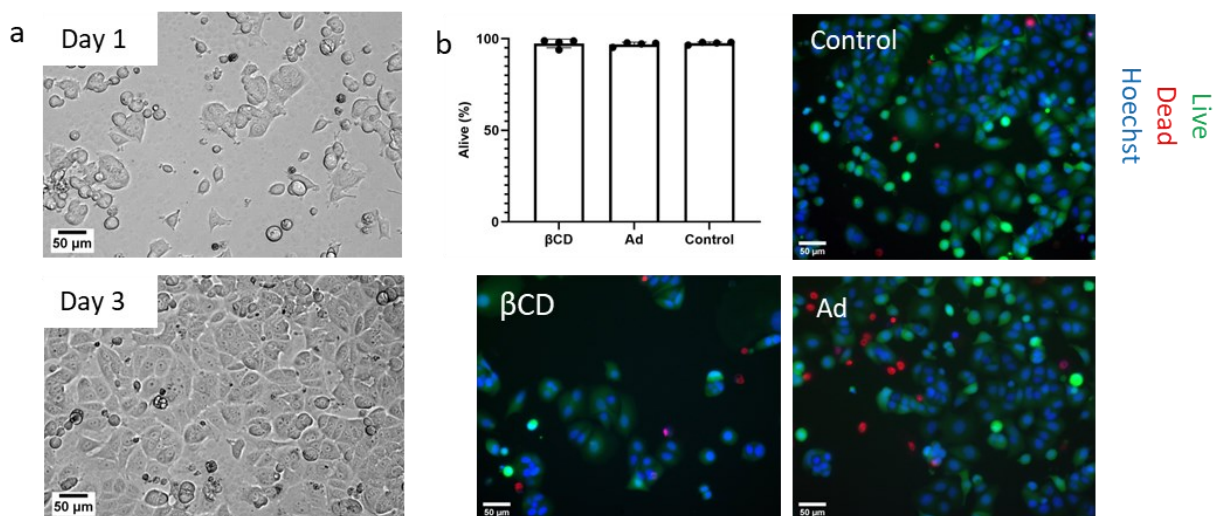


Figure 17: Live/dead study of guest and host granules. a) Growth of MCF7 breast cancer cells over 3 days, plated with β CD functionalized beads. b) comparison of live/dead staining results for MCF7 cells with β CD functionalized beads, Ad functionalized beads, and a control of no beads.

Cultures were created using T47D cell aggregates to study the growth of spheroids in the packed granular hydrogels and create growth curves over a 6-day time period. Four conditions were chosen for the granular gels, as laid out in table 2, to capture a range of plastic and elastic properties.

Table 2: Fabrication parameters used for packed granular gels in T47D aggregate cultures.

AAm%/Bis% (w/v)	Vortex Time (s)	Ad Concentration (mg/ml)	β CD Concentration (mg/ml)	Elastic Modulus, (Pa) (Figure 16)	Yield Stress (Pa) (Figure 16)	Nominal Storage Modulus (E)/ Yield Stress (Y)
3/0.1	120	0.4	24	70 ± 16	41 ± 18	E=70,Y=40
3/0.1	120	0.8	24	85 ± 8	68 ± 10	E=85,Y=70
3/0.1	120	4	24	204 ± 12	108 ± 8	E=200,Y=110
7.5/0.05	120	4	24	962 ± 89	371 ± 121	E=960,Y=370

A TrueGel3D non-cell degradable and non-plastically deformable control was chosen to observe T47D aggregate growth in a linear elastic environment over a range of elastic moduli. Crosslinking strengths were chosen of 1.5, 2, 3, and 4 according to the supplier technical information corresponding with an elastic moduli of 30 Pa, 100 Pa, 300 Pa and 1000 Pa, respectively.

Highest growth in TrueGel3D conditions was seen for the lowest gel stiffness of 30 Pa leading to a doubling in the area by day 6 (Figure 18). As gel stiffness increased to 100 Pa, mean normalized growth decreased to 1.75 on day 6, and further down to 1.58 times for stiffnesses of 300 and 1000 Pa. Increased cell density was also observed in all conditions, as seen by the formation of darker regions within the aggregate from day 3 to day 6. Consistent growth was observed for all gel conditions.

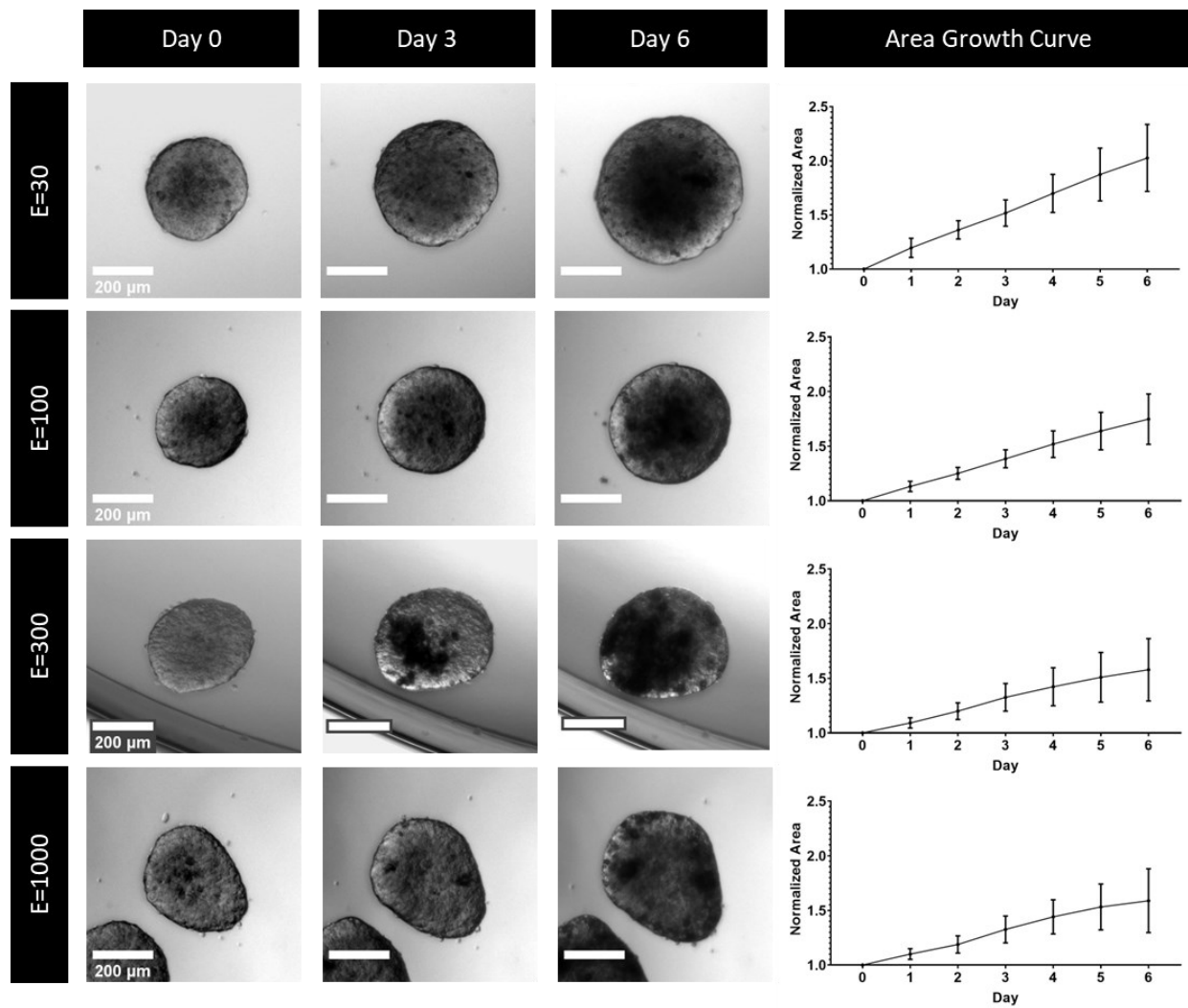


Figure 18: T47D growth in TrueGel hydrogels. Growth of T47D aggregates over 6 days in linear elastic TrueGel3D gels for elastic moduli of 30 Pa, 100 Pa, 300 Pa, and 1000 Pa. Growth curves are of aggregate normalized area with respect to original day 0 area. E = storage modulus (Pa).

Similarly, the highest growth in the packed granular gels was seen for granular gels with the lower stiffness and lower yield stress ($E=70, Y=40$), with mean normalized area of the aggregates reaching up to 1.78 (Figures 19). Lowest growth was seen in packed gels with the highest stiffness and yield stress ($E=960, Y=370$), with a mean of 1.38 normalized area on day 6. Slightly higher growth was seen for the softer gels with high yield ($E=200, Y=110$), for a mean normalized area of 1.55.

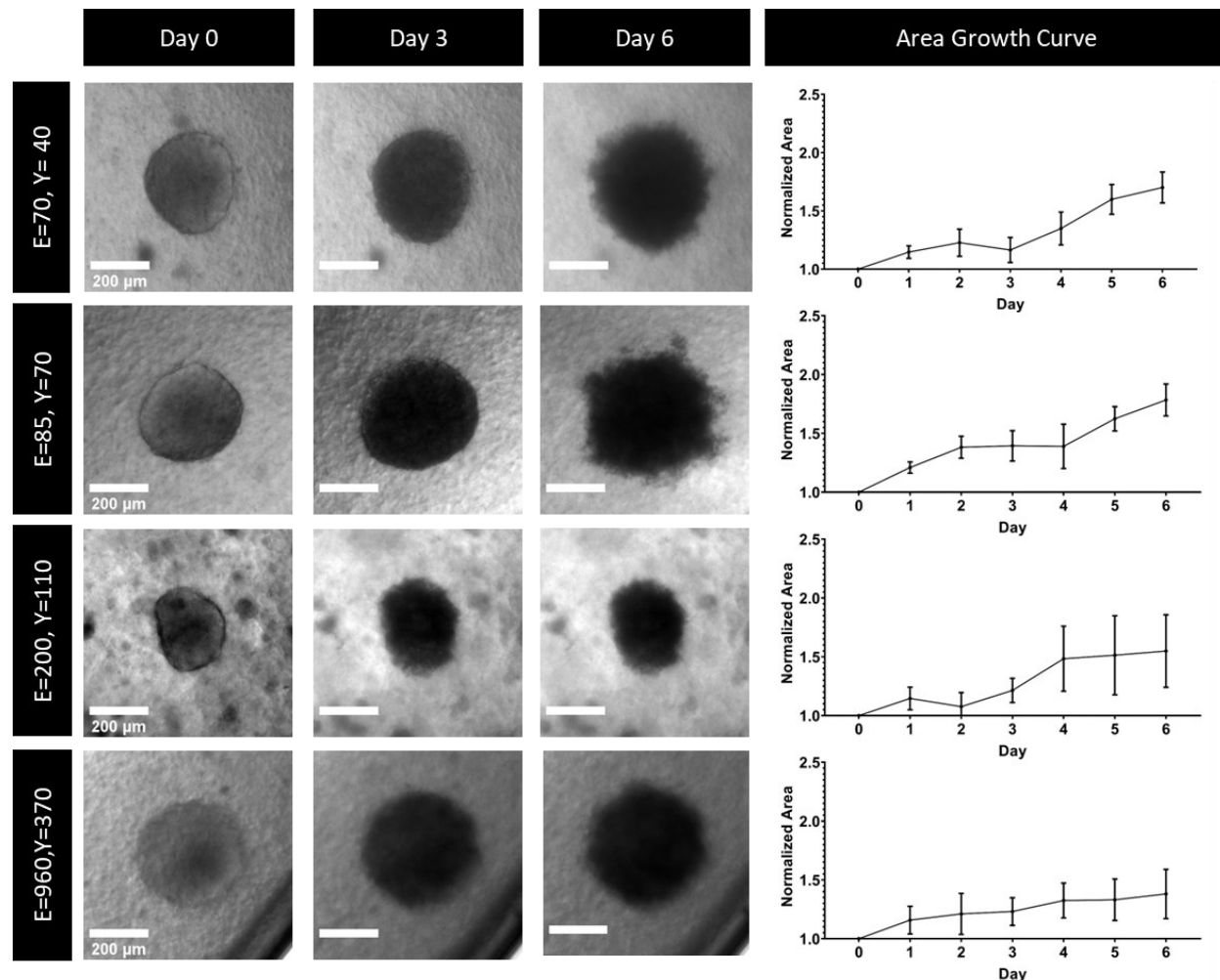


Figure 19: T47D growth in packed granular guest-host hydrogels. Growth of T47D aggregates over 6 days in packed granular hydrogels. Samples varied for Ad concentration, and individual bead stiffness. Growth curves are of aggregates normalized area with respect to original day 0 area. E = storage modulus (Pa), Y = yield stress (Pa).

Comparisons of aggregate day 6 growth were completed for both TrueGels and packed granular hydrogels, and statistical analysis was performed (Figure 20a). Across the TrueGel platform, a statistical difference was found between gels of 30 Pa and that of 300 and 1000 Pa for overall growth of the aggregates with regard to the differing gel stiffnesses. However, no significant differences were found for the gel of 100 Pa. Comparison of the aggregate's day 6 growth for the packed granular gels showed a statistical difference between the E=70,Y=40 and E=85,Y=70 with that of the E=960,Y=370 (Figure 20b). However, there were no significant differences for beads of E=200,Y=110.

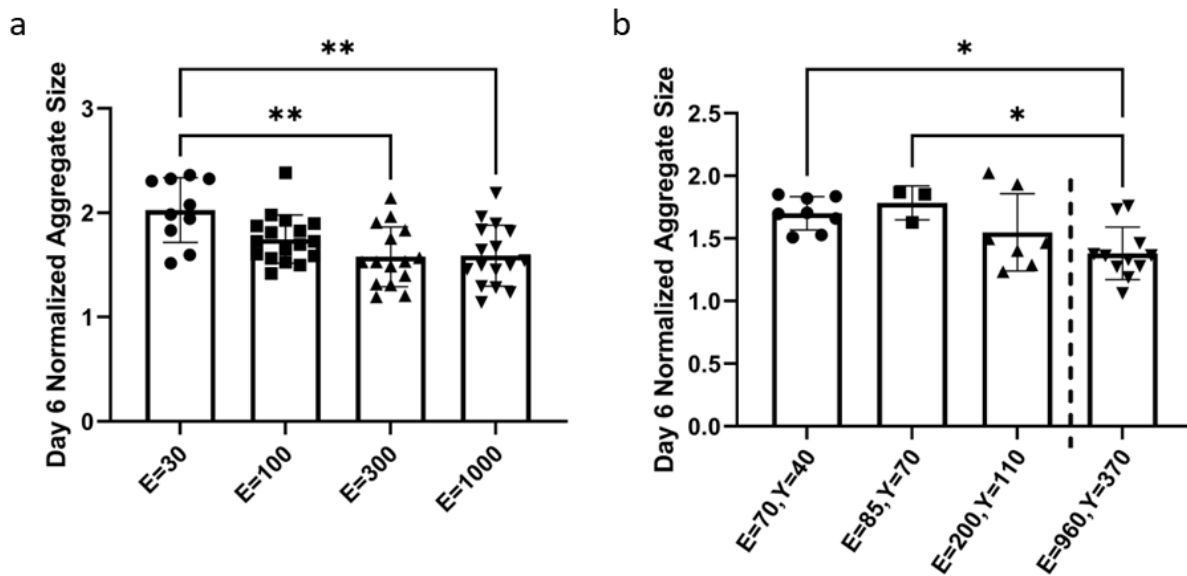


Figure 20: Day 6 T47D aggregate growth. Comparison of a) different TrueGel storage modulus and b) different packed gel formulations for day 6 aggregate growth. For packed gels, Ad concentration increases over the first three (L to R), while individual bead formulation is consistent. The last two conditions have the same level of Ad functionality, but the 4th condition is a stiffer formulation. E = storage modulus (Pa), Y = yield stress (Pa). * = p < 0.05, ** = p < 0.01.

Invasiveness was measured using circularity for aggregates in TrueGels of E=100 and E=1000 as a comparison of low and high stiffnesses, as well as all packed gel conditions to examine a range of yield stresses. For both TrueGel conditions, circularity was found to be close to 1 and consistent over the 6-day period, between 1.02 and 1.03 for E=100 and 1.04 and 1.06 for E=1000, (Figure 21). No significant day-to-day differences were determined for either TrueGel's condition over the course of the experiment, confirming a lack of invasion into the hydrogel.

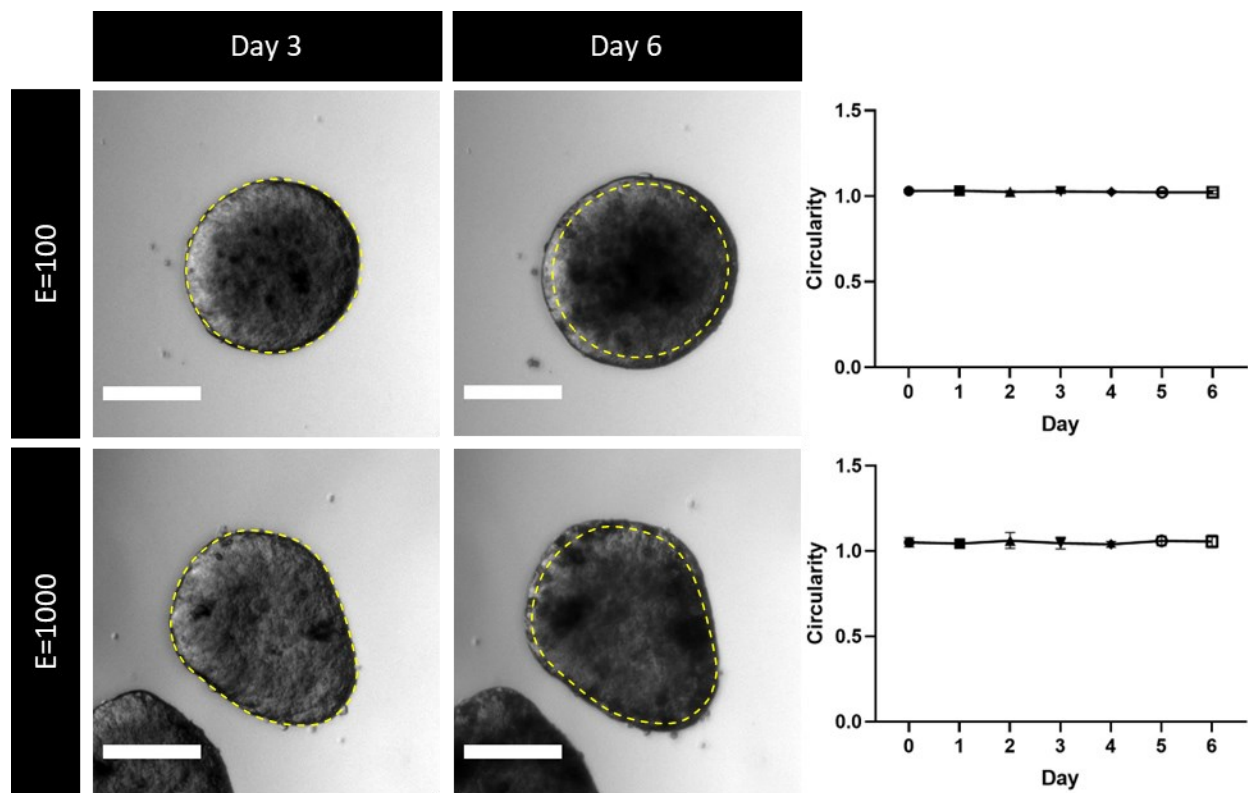


Figure 21: Invasion of T47D aggregates in TrueGel hydrogels. Outline of aggregate perimeter on day 3 and overlay of the perimeter on day 6 aggregate for visualization of invasion, as well as plots of aggregate invasiveness measured through their circularity. Values close to 1 represent a perfectly circular aggregate cross-sectional area, and values above 1 indicate a deviation from the circular shape. No significance was found in the measured aggregate circularity. E = storage modulus (Pa).

The packed bead hydrogels of E=70, Y=40 had an initial circularity of 1.05 with a significant increase from 1.08 to 1.21 between days 2 and 3, and further to 1.68 by day 4 indicating invasion of the aggregate starting and progressing through the packed beads. The E=85, Y=70 gels had an initial circularity of 1.03 and increased significantly to 1.43 between days 3 and 4, again showing invasion of the aggregate into the surrounding ECM. The packed bead hydrogels of E=200, Y=110 and E=960, Y=370 showed a higher overall circularity of 1.08 to 1.24 and 1.12 to 1.22 respectively, but no significant day-to-day change was found indicating no invasion into the surrounding gels (Figure 22).

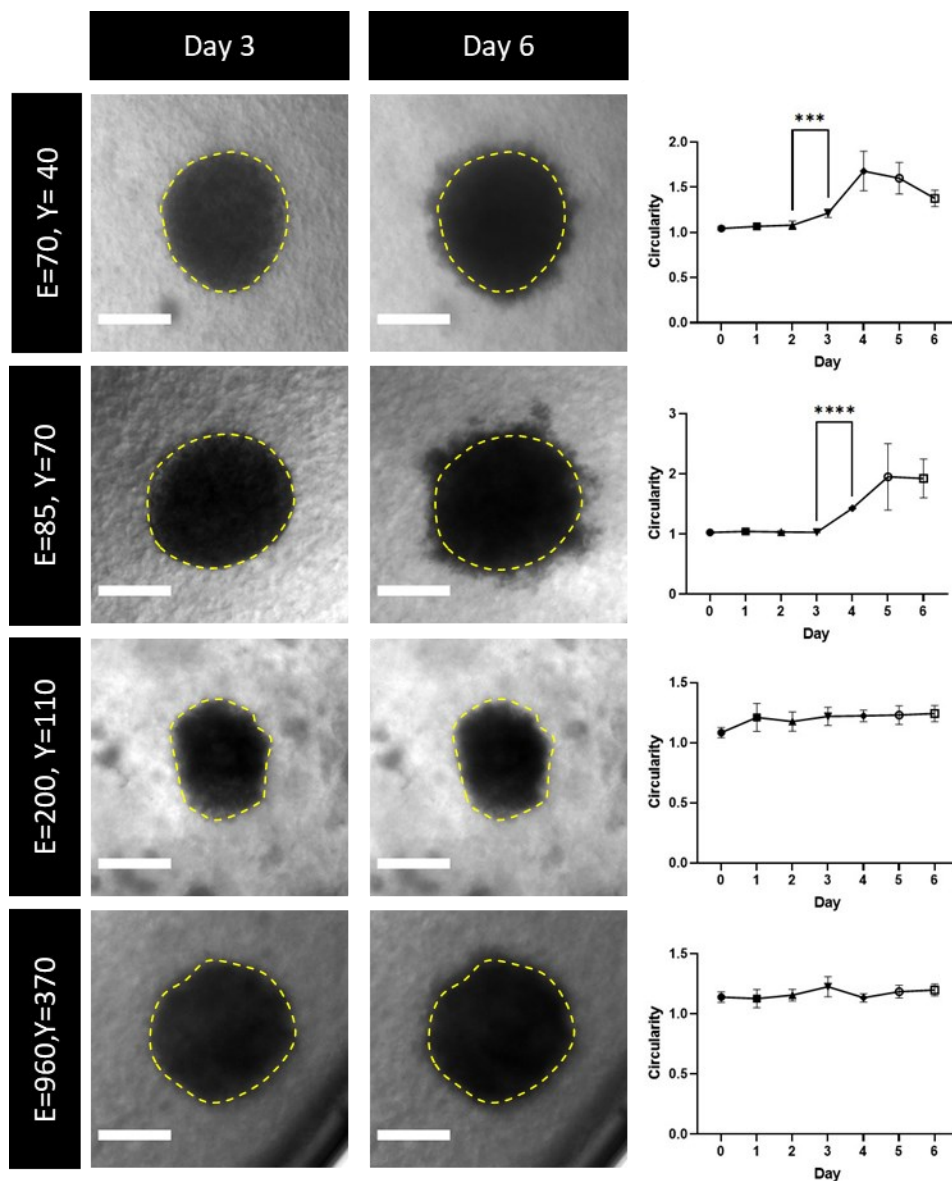


Figure 22: Invasion of T47D aggregates in packed granule guest-host hydrogels. Outline of aggregate perimeter on day 3 and overlay of the perimeter on day 6 aggregate for visualization of invasion, as well as plots of aggregate invasiveness measured through their circularity. Values close to 1 represent a perfectly circular aggregate cross-sectional area, and values above 1 indicate a deviation from the circular shape. E = storage modulus (Pa) Y = yield stress (Pa). *** = $p < 0.001$, **** = $p < 0.0001$.

6 Discussion

Design of a plastically tunable hydrogel system required the study and understanding of the different controllable properties. Since this is a packed microgel system, those include properties inherent to individual granules. Size of individual granules was shown to be influenced by the fabrication parameters, in this case the length of time the emulsion was vortexed for during gelation (Figure 9a). However, even for the shortest vortex times, which is 5 seconds, the mean bead size was still quite small at roughly 30 μm in diameter when compared to the 10 μm diameter for the 120 second vortex time. This is most likely accounted for by the stir plate RPMs influencing the size after the vortexing but during the gelation process. The fabrication of larger beads would require a lower stir plate speed than used in this work. If smaller beads were needed other methods would have to be explored, as increasing vortex time leads to a diminishing returns effect for the size. Sonication could be one method to fabricate nano scale beads. Recovery of granules also proved more difficult as size decreased due to slower settling times and had an increased likelihood of wasting beads during subsequent washing steps. The addition of βCD or Ad did not significantly change the bead size in comparison to the pure PAAm granules when added at their maximum solubility during the pre-gel set up (Figure 9b), although measurements were taken only at 120 second vortex time and inclusion of these functionalities may have a more pronounced influence in larger beads.

Initial fluorescent intensity test of the functionalized Ad or βCD beads using the guest-host dyes showed plateaus of intensity at higher concentrations for both (Supplementary Figure 21) leading to the selection of lower concentrations to functionalize the beads. Successful bead functionalization at different concentrations was visualized by the additions of the appropriate guest or host dye under fluorescent imaging (Figure 10). Not only does it show the different degrees of functionality, but it shows the success of dissolving Ad-AAm into the kerosene phase directly can provide functionalization through random interactions with the pre-gel solution. This was required as Ad has poor solubility in aqueous solutions but is soluble in hydrocarbons. Measurements were taken for beads of 3/0.1 AAm/Bis (w/v%) and for a vortex time of 120 seconds, but the beads stiffness and size may play a role in the level of functionalization and would need to be characterized further.

As established by Pelham and Wang, varying the amount of AAm and Bisacrylamide in the pre-gel solution can adjust the hydrogels stiffness⁷⁰. The selected gel formulations covered a range of biologically relevant stiffnesses from tens of pascals, up to a few kilopascals in range, and were confirmed using shear rheometry (Figure 11). While the measurements were taken on conventional bulk gels, it was assumed that beads of the same formulation would be of similar stiffness. However, the three studied bead properties, that is the size, stiffness, and guest or host functionalization, would most likely be interlinked. For example, increasing the beads stiffness with the pre-gel formulation would lead to quicker gelation which would influence the size of the beads during vortexing, or the addition of Ad or β CD could affect the mechanical properties of the hydrogels after gelation. The intertwining of these three properties means that characterization of the chosen size, stiffness, and functionalization is required for combinations not studied in this work.

Creation of this biomaterial required ensuring that the guest-host interlinking between beads was occurring as expected. Packing together of the gel only occurred when functionalized beads were combined with one another, and not with unfunctionalized PAAm (Figure 12), and showed high affinity for bead-to-bead interlinking, with gels deforming into each other due to the strength of the guest-host interactions (Figure 13). Binding together of beads to form a packed gel was found to be almost instantaneous, where if a high concentration of one bead type was added to the other, also at a high concentration, the packed gel would form within the suspension instantaneously. This required the handling and mixing of the beads at low concentrations ($< 100 \mu\text{L beads/ml}$) to ensure adequate distribution of bead types and uniform properties through the packed gel. Development of a plastic hydrogel platform requires that the structure be maintained after the deformation has occurred, meaning that the guest-host bonds need to be reformed in new configurations after being broken apart. Up to 15 bindings and separations of the Ad bead on the β CD bulk gel showed similar deformation of the bead before breaking of the guest-host complexes (Figure 15b). In the context of biomaterials, it is not known exactly how often this breaking and reforming would need to occur to allow for the plastic remodeling of the ECM and growth of aggregates or cell migration. However, no signs of

weakening adhesion were seen over repeated tests, indicating this platform would properly allow for this type of behaviour.

This granule-hydrogel platform allows for control over the stiffness of the material as a measure of its elasticity, as well as its yield stress for when the biomaterials moves from the elastic into the plastic deformation region. This was accomplished through adjustments to the packed gel granule size, individual bead stiffness, and the level of guest and host functionalization. As decreased yield stress and strain were observed with smaller bead sizes, it may be due to the changing ratio of guest-host bead-to-bead interlinking to crosslinking within individual PAAm gels. That is, if the granules are larger then crosslinking within the beads would play more of a role within the packed gels, where with smaller individual gels the guest-host interlinking would provide more to the structure and in turn be more influential on the yielding of the material.

When looking at the effects of individual bead stiffness on the packed gel, both storage modulus and yield stress increased with stiffness (Figure 16b). Interestingly, for both 3/0.1 and 7.5/0.05 AAm/Bis (w/v%) formulations the packed gel had a lower bulk stiffness than the conventional bulk gel of the same formulation, while the softer 3/0.05 formulation had a slightly stiffer granule gel than conventional PAAm hydrogel. Further study would be required to understand if the packed gel stiffness translates to the local stiffness that would be seen by cells or aggregates. It was also observed that while yield stress increases with bead stiffness, the yield strain decreases, believed to be due to the increased resistance to deformation of stiffer beads before the guest-host interlinking breaks.

Changing the level of guest or host functionalization showed that decreasing either leads to a decrease in both packed gel storage modulus and the yield stress (Figures 16 c, d). This is believed to occur due to lower bead-to-bead interlinking reducing the mechanical stiffness of the packed gel and requiring less stress in breaking the guest-host complexes. Interestingly, similar yield strains were required for the various levels of guest or host functionalization, indicating that beads were deformed a similar amount regardless of the required force to separate the guest-host complexes.

When applied to cell cultures, no differences in cell viability were observed, and the two types of functionalized beads did not appear to hinder or slow cell proliferation. It was also observed that the cells did not adhere to either set of beads. While PAAm is inherently non-adhesive to cells and can be adhesively functionalized through the surface binding of sulfoSANPHA and collagen, it was not known if the addition of Ad or β CD would change the cells interaction with the beads or allow for adhesion. This positions the packed gel to study cell and aggregate behaviour in a non-adhesive environment.

T47D aggregates encapsulated in TrueGels showed growth for all the ECM stiffnesses tested (Figure 18). As expected, the lower stiffness gels led to higher expansion of the aggregates. What was not observed was a complete plateau in growth for any of the TrueGel conditions, that is confinement of the aggregate due to a limit in the allowable elastic deformation. For the lower stiffnesses of 30 and 100 Pa, a linear increase of aggregate area was seen over the 6 days in culture. For the higher TrueGel stiffnesses of 300 and 1000 Pa, growth was seen to slow by day 5. Similar growth rates were seen for both 300 and 1000 Pa. A statistically significant difference was found between the 30 Pa and the 300 and 1000 Pa stiffnesses, confirming that the elasticity of the ECM plays a role in limiting T47D aggregate growth rate. As this TrueGel platform is non-degradable from cells and is non-plastically deformable, no signs of invasion or sprouting from the aggregate were observed as there was no significant change in the aggregate's circularity over time for the two conditions considered, that is the $E=100$ and $E=1000$. The effect of the platform's elasticity can be used as a comparison for growth to that of the packed gels.

Similar to the TrueGels, the packed granular gels showed higher rates of growth for combinations with lower storage modulus (Figure 19). However, two conditions were at play in the packed gels, that being the stiffness of the individual beads and the level of interlinking due to Ad functionalization, leading to a range for both the storage modulus and the yield point. The first three conditions, $E=70, Y=40$, $E=85, Y=70$, and $E=200, Y=110$, were created with the same bead formulation (3/0.1 AAm/Bis (w/v%)) but differing concentrations of Ad in the pre-gel, 0.4, 0.8, and 4 mg/ml respectively, while the last gel has an Ad concentration of 4 mg/ml but a gel formulation of 7.5/0.05 AAm/Bis (w/v%). The two lowest stiffness and yield points had not only higher growth but also showed signs of cell invasion into the packed gel by day 6 as observed by

the branching out of cells into the gel and measured by the change in the aggregate's circularity. The E=200, Y=110 and E=960, Y=370 gels did not show the same signs of invasion and there was no significance found in the day-to-day circularity of the samples. As the guest-host interactions cause binding and deformation of the beads when packed together, the porosity would be limited, and as the PAAm are non-cell-degradable, this invasion of the T47D aggregate is believed to be due to plastic remodeling of the ECM via the breaking of the guest-host bead interlinking. First signs of invasion in the low yield packed gels occur between days 2 and 3 for E=70, Y=40 and between days 3 and 4 for E=85, Y=70. This indicates that invasion into the ECM will occur earlier due to lower hydrogel yield stress. As the TrueGel E=100 with a similar stiffness did not show invasion indicating that this behaviour is dependent on the plastic properties of the gel. However, as the E=200, Y=110 packed gel did not show invasion, this suggests that there is a limit to the materials plastic properties where the yield point is so high that the materials behaviour is similar to the purely elastic TrueGels. A longer timeframe experiment would be required to explore when breaking of the guest-host bonds would occur for the higher yield point packed gels, such as the E=200, Y=110 or even then E=960, Y=370, or if the bead-to-bead interlinking strength threshold is above the stress that the aggregate could generate. Decreasing aggregate growth was seen as both packed gel elasticity and yield points increased, however the same behaviour was observed in TrueGels where yield points were not a factor. While a significant difference is measured between the low yield, low stiffness packed gels of E=70, Y=40, and E=85, Y=70 and the high interlinking high stiffness gel of E=960, Y=370, further work would need to be completed to understand the role plasticity plays in overall growth, if yield stress alone could be enough to limit growth rates in soft gels, or if aggregate growth is regulated by the elasticity independently of the materials plasticity.

7 Directions for Future Work

The presented work lays out a foundation to build upon for the use of a packed granular hydrogel with tunable plastic deformation properties. However, much more work will be needed to further characterize it, explore its limitations, and understand how to apply it to cell and aggregate cultures. Fabrication of larger and smaller granules would be needed to further understand how this property influences packed gel mechanical properties. Not only that, but other combinations of bead stiffness, sizes, and levels of functionalization should be explored to better understand the complex relationship between these three properties and the corresponding elasticity and plasticity. For example, adjusting the bead formulation to increase the stiffness would lead to faster gelation of the beads, which in turn would affect the size of the beads. It is also of note that in this work the size of the beads was characterized for just one formulation with varying vortex times. To completely rule out the effect of bead sizes on the mechanical properties of different packed gel bead formulations, vortex times and corresponding bead size distributions should be characterized for a range of microgel stiffness, and then beads of similar sizes could be compared. Varying the ratio of Ad to β CD functionalized beads could also be studied as a method of controlling the packed gel properties.

While the study of the bulk packed gel properties was completed, further work would be needed to explore the local behaviour of the gel. This could include individual bead stiffness and the stresses observed by encapsulated tissues and cells. Osmotic pressure testing could be used to confirm that the measured stiffness for different formulations of PAAm translates from the conventional bulk gel down to the individual granules fabricated using the emulsion method, and that the addition of Ad or β CD or changing the granule size does not significantly change the resulting storage modulus. Local packed gel stiffness could also be probed via the use of thermally responsive hydrogel probes, such as those presented by Mok et al. ¹⁶⁰, where the thermal expansion of the probe would allow for a better understanding of not only the local stiffness but the required local yield stress at the cell and tissue scale.

Long-term stability of the packed gels mechanical properties should also be explored. The effects of cell media are not known on bead-to-bead interlinking and could reduce the hydrogels elastic

and plastic properties over time by interacting with the guest or host molecules and reducing the available binding sites. However, a reduction in bead-to-bead interlinking and breaking apart of the packed gel was not seen during the course of this work while in culture media. While the work here presented a non-adhesive aggregate culture study, further development of the packed beads would be required to allow for the cell adhesion. This would require a fabrication method that incorporates binding sites without blocking the guest or host functionalities, which is especially difficult as β CD is non-selective in the guest molecule they will uptake. A co-polymer hydrogel could be one method to include adhesive sites without hindering the guest-host functionalization.

Eventual work with this platform will look to apply it to further aggregate studies where the yield point could be varied while maintaining the same mechanical elasticity. In this way, the role that plastic deformation plays in tissue behaviour could be further explored independently of the ECMs elasticity. This would be key in understanding how a materials yield point affects aggregate growth but could also include its influence on cell migration, proliferation, tissue growth, and invasiveness. Maximum yield point limits for specific aggregate types could also be explored. More specifically, the yield point and plasticity could be studied for its role in disease and cancer progression, such as tumor metastasis. Additionally, while it is known that stem cell decision can be controlled through the elasticity of the ECM, this platform has the potential to study how plasticity of the ECM would contribute to these cell fate choices through the encapsulation of organoids in the presented packed granular gels. However, more advanced methods for imaging the encapsulated tissues and cells would be required as one of the largest drawbacks of this system is the poor resolution caused by the packed together granules. Techniques such as confocal imaging could prove useful.

Applications for guest and host functionalized beads can go beyond a packed gel system. One potential use includes 3D printing of ECM scaffolds, where spatial control of bead mixing would allow for the creation of soft hydrogel structures. Alternatively, a 3D print-in-bath approach could be taken, where an extrusion needle prints one set of beads into a suspension bath of the other. The micromanipulation techniques used to explore reattachment of the gels could further be developed to allow these beads to be sensors of the guest-host binding strength. Where the

known speed of the manipulator and stiffness of the beads would allow for modeling of the forces required to separate the guest-host complexes.

8 Conclusions

In this work, the tuning and development of a plastically deformable packed granular hydrogel platform was completed for application in cell cultures and tissue engineering. Successful fabrication of guest and host functionalized granule hydrogels was completed through a two-phase vortex emulsion process. Control of the granule properties, which is size, stiffness, and levels of guest and host functionalization, was shown to be possible through adjustment of the pre-gel formulation and fabrication steps. Repeated guest-host binding was shown without any potential loss of adhesion due to repeated breaking of the complex. When packing the microgels together, tuning of their mechanical elasticity and yield point transition to the plastic region was successful through adjusting the granule properties. It was found that adjusting the granule size had an insignificant effect on the packed gel storage modulus and that decreasing bead size played a small role in decreasing the yield stress. Increasing the individual bead stiffness led to an increase in both the packed gels storage modulus and yield stress but was inversely related to the yield strain. Reducing the bead-to-bead interlinking, through reduction of Ad or β CD functionality showed both a reduction in the bulk gel storage modulus and its yield stress while maintaining the same yield strain.

In cell studies, the guest and host functionalized beads showed no adverse effects towards cell behaviour or proliferation. High cell viability was maintained when compared to the control. The granular nature of the gel allowed for easy encapsulation of cells and aggregates. Application of the packed gel platform to T47D breast cancer aggregates showed growth for a range of stiffnesses and yield stresses, with a higher aggregate growth rate for lower measured storage moduli. Interestingly, aggregate invasion was observed in packed gels of beads with lower Ad functionalization, and in turn a lower yield stress, showing breaking of the bead-to-bead guest-host interlinking and remodeling of the ECM due to increased stress applied from the growing aggregates.

The proposed packed granular hydrogel platform lays the foundation for studying and understanding ECM plasticity and its relationship to tissue growth and behaviour. Further work will be required to characterize the limits of this biomaterial and explore its packed gel properties

for varying combinations of granule sizes, stiffnesses, and guest and host functionalization. The long-term stability of the system, as well as its tissue-level mechanical environment, could further be investigated. Development of this platform would allow for deeper insight into mechanical signaling in disease progression and for its role in stem cell fate decisions, providing a platform of low mechanical variability with control over both its elasticity and plasticity as an alternative to commonly used materials such as Matrigel. The unique behaviour of this granular biomaterial could also be applied elsewhere, such as 3D printing techniques for soft hydrogel scaffolds. Overall, this platform and its continued development and application is on the cusp of an emerging class of exciting granule-based biomaterials for tissue engineering.

9 References

1. Kim, J., Koo, B.-K. & Knoblich, J. A. Human organoids: model systems for human biology and medicine. *Nat. Rev. Mol. Cell Biol.* **21**, 571–584 (2020).
2. Li, H. *et al.* To Better Generate Organoids, What Can We Learn from Teratomas? *Front. Cell Dev. Biol.* **9**, 700482 (2021).
3. Vanderburgh, J., Sterling, J. A. & Guelcher, S. A. 3D Printing of Tissue Engineered Constructs for In Vitro Modeling of Disease Progression and Drug Screening. *Ann. Biomed. Eng.* **45**, 164–179 (2017).
4. Wood, J. A., Liliensiek, S. J., Russell, P., Nealey, P. F. & Murphy, C. J. Biophysical Cueing and Vascular Endothelial Cell Behavior. *Materials* **3**, 1620–1639 (2010).
5. Hughes, C. S., Postovit, L. M. & Lajoie, G. A. Matrigel: a complex protein mixture required for optimal growth of cell culture. *Proteomics* **10**, 1886–1890 (2010).
6. Golman, J. M., Weinand, P. & Mooney, D. J. Extracellular matrix plasticity as a driver of cell spreading. *Proc. Natl. Acad. Sci. U. S. A.* **117**, 25999–26007 (2020).
7. Chaudhuri, O., Cooper-White, J., Janmey, P. A., Mooney, D. J. & Shenoy, V. B. Effects of extracellular matrix viscoelasticity on cellular behaviour. *Nature* **584**, 535–546 (2020).
8. Bissell, M. J. & Barcellos-Hoff, M. H. The Influence of Extracellular Matrix on Gene Expression: Is Structure the Message? *J. Cell Sci.* **1987**, 327–343 (1987).
9. Adil, M. M. *et al.* Efficient generation of hPSC-derived midbrain dopaminergic neurons in a fully defined, scalable, 3D biomaterial platform. *Sci. Rep.* **7**, 40573 (2017).
10. Puig-Sanvicens, V. A. C., Semino, C. E. & zur Nieden, N. I. Cardiac differentiation potential of human induced pluripotent stem cells in a 3D self-assembling peptide scaffold. *Differentiation* **90**, 101–110 (2015).
11. DuChez, B. J., Doyle, A. D., Dimitriadis, E. K. & Yamada, K. M. Durotaxis by Human Cancer Cells. *Biophys. J.* **116**, 670–683 (2019).

12. Wolf, K. *et al.* Physical limits of cell migration: Control by ECM space and nuclear deformation and tuning by proteolysis and traction force. *J. Cell Biol.* **201**, 1069–1084 (2013).
13. Alberts, B. *Molecular Biology of the Cell.* (W.W. Norton & Company, 2017). doi:10.1201/9781315735368.
14. Grossman, M. *et al.* Tumor Cell Invasion Can Be Blocked by Modulators of Collagen Fibril Alignment That Control Assembly of the Extracellular Matrix. *Cancer Res.* **76**, 4249–4258 (2016).
15. Lv, H. *et al.* Biomaterial stiffness determines stem cell fate. *Life Sci.* **178**, 42–48 (2017).
16. Bertucci, T. B. & Dai, G. Biomaterial Engineering for Controlling Pluripotent Stem Cell Fate. *Stem Cells Int.* **2018**, 1–12 (2018).
17. Zoldan, J. *et al.* The influence of scaffold elasticity on germ layer specification of human embryonic stem cells. *Biomaterials* **32**, 9612–9621 (2011).
18. Leipzig, N. D. & Shoichet, M. S. The effect of substrate stiffness on adult neural stem cell behavior. *Biomaterials* **30**, 6867–6878 (2009).
19. Lantoine, J. *et al.* Matrix stiffness modulates formation and activity of neuronal networks of controlled architectures. *Biomaterials* **89**, 14–24 (2016).
20. Rowlands, A. S., George, P. A. & Cooper-White, J. J. Directing osteogenic and myogenic differentiation of MSCs: interplay of stiffness and adhesive ligand presentation. *Am. J. Physiol.-Cell Physiol.* **295**, C1037–C1044 (2008).
21. Sun, M. *et al.* Extracellular matrix stiffness controls osteogenic differentiation of mesenchymal stem cells mediated by integrin $\alpha 5$. *Stem Cell Res. Ther.* **9**, 52 (2018).
22. Choi, B. *et al.* Stiffness of Hydrogels Regulates Cellular Reprogramming Efficiency Through Mesenchymal-to-Epithelial Transition and Stemness Markers. *Macromol. Biosci.* **16**, 199–206 (2016).
23. Kim, D. *et al.* Physicochemical Properties in 3D Hydrogel Modulate Cellular Reprogramming into Induced Pluripotent Stem Cells. *Adv. Funct. Mater.* **31**, 2007041 (2021).

24. Blin, G. *et al.* Nano-scale control of cellular environment to drive embryonic stem cells selfrenewal and fate. *Biomaterials* **31**, 1742–1750 (2010).
25. Perez, R. A. *et al.* Biomaterials control of pluripotent stem cell fate for regenerative therapy. *Prog. Mater. Sci.* **82**, 234–293 (2016).
26. Tian, H., Shi, H., Yu, J., Ge, S. & Ruan, J. Biophysics Role and Biomimetic Culture Systems of ECM Stiffness in Cancer EMT. *Glob. Chall.* **6**, 2100094 (2022).
27. Wang, M. *et al.* Effect of three-dimensional ECM stiffness on cancer cell migration through regulating cell volume homeostasis. *Biochem. Biophys. Res. Commun.* **528**, 459–465 (2020).
28. Nuhn, J. A. M., Perez, A. M. & Schneider, I. C. Contact guidance diversity in rotationally aligned collagen matrices. *Acta Biomater.* **66**, 248–257 (2018).
29. Tozluoğlu, M. *et al.* Matrix geometry determines optimal cancer cell migration strategy and modulates response to interventions. *Nat. Cell Biol.* **15**, 751–762 (2013).
30. Tang, M. *et al.* Rapid 3D Bioprinting of Glioblastoma Model Mimicking Native Biophysical Heterogeneity. *Small* **17**, 2006050 (2021).
31. Ondeck, M. G. *et al.* Dynamically stiffened matrix promotes malignant transformation of mammary epithelial cells via collective mechanical signaling. *Proc. Natl. Acad. Sci.* **116**, 3502–3507 (2019).
32. Patwardhan, S., Mahadik, P., Shetty, O. & Sen, S. ECM stiffness-tuned exosomes drive breast cancer motility through thrombospondin-1. *Biomaterials* **279**, 121185 (2021).
33. Maller, O. *et al.* Tumor-associated macrophages drive stromal cell-dependent collagen crosslinking and stiffening to promote breast cancer aggression. *Nat. Mater.* **20**, 548–559 (2021).
34. Paszek, M. J. *et al.* Tensional homeostasis and the malignant phenotype. *Cancer Cell* **8**, 241–254 (2005).
35. Lubliner, J. *Plasticity Theory*. (Courier Corporation, 2008).

36. Buchmann, B. *et al.* Mechanical plasticity of collagen directs branch elongation in human mammary gland organoids. *Nat. Commun.* **12**, 2759 (2021).
37. Nam, S., Lee, J., Brownfield, D. G. & Chaudhuri, O. Viscoplasticity Enables Mechanical Remodeling of Matrix by Cells. *Biophys. J.* **111**, 2296–2308 (2016).
38. Mohammadi, H., Arora, P. D., Simmons, C. A., Janmey, P. A. & McCulloch, C. A. Inelastic behaviour of collagen networks in cell–matrix interactions and mechanosensation. *J. R. Soc. Interface* **12**, 20141074 (2015).
39. Kim, J. *et al.* Stress-induced plasticity of dynamic collagen networks. *Nat. Commun.* **8**, 842 (2017).
40. Malandrino, A., Trepats, X., Kamm, R. D. & Mak, M. Dynamic filopodial forces induce accumulation, damage, and plastic remodeling of 3D extracellular matrices. *PLOS Comput. Biol.* **15**, e1006684 (2019).
41. Liu, A. S. *et al.* Matrix viscoplasticity and its shielding by active mechanics in microtissue models: experiments and mathematical modeling. *Sci. Rep.* **6**, 33919 (2016).
42. Paul, C. D., Mistriotis, P. & Konstantopoulos, K. Cancer cell motility: lessons from migration in confined spaces. *Nat. Rev. Cancer* **17**, 131–140 (2017).
43. Harada, T. *et al.* Nuclear lamin stiffness is a barrier to 3D migration, but softness can limit survival. *J. Cell Biol.* **204**, 669–682 (2014).
44. Sabeh, F., Shimizu-Hirota, R. & Weiss, S. J. Protease-dependent versus -independent cancer cell invasion programs: three-dimensional amoeboid movement revisited. *J. Cell Biol.* **185**, 11–19 (2009).
45. Lee, H., Gu, L., Mooney, D. J., Levenston, M. E. & Chaudhuri, O. Mechanical confinement regulates cartilage matrix formation by chondrocytes. *Nat. Mater.* **16**, 1243–1251 (2017).
46. Wisdom, K. M. *et al.* Covalent cross-linking of basement membrane-like matrices physically restricts invasive protrusions in breast cancer cells. *Matrix Biol.* **85–86**, 94–111 (2020).

47. Jia, Y. *et al.* The Plasticity of Nanofibrous Matrix Regulates Fibroblast Activation in Fibrosis. *Adv. Healthc. Mater.* **10**, e2001856 (2021).
48. Buchmann, B., Fernández, P. & Bausch, A. R. The role of nonlinear mechanical properties of biomimetic hydrogels for organoid growth. *Biophys. Rev.* **2**, 021401 (2021).
49. Razavi, M. *Biomaterials for Tissue Engineering*. (Bentham Science Publishers, 2017).
50. Ma, L. *et al.* Collagen/chitosan porous scaffolds with improved biostability for skin tissue engineering. *Biomaterials* **24**, 4833–4841 (2003).
51. Kołodziejaska, M., Jankowska, K., Klak, M. & Wszola, M. Chitosan as an Underrated Polymer in Modern Tissue Engineering. *Nanomater. Basel Switz.* **11**, 3019 (2021).
52. Chu, Y. *et al.* Long-term stability, high strength, and 3D printable alginate hydrogel for cartilage tissue engineering application. *Biomed. Mater. Bristol Engl.* **16**, (2021).
53. Shafei, S. *et al.* Exosome loaded alginate hydrogel promotes tissue regeneration in full-thickness skin wounds: An in vivo study. *J. Biomed. Mater. Res. A* **108**, 545–556 (2020).
54. Kleinman, H. K. & Martin, G. R. Matrigel: basement membrane matrix with biological activity. *Semin. Cancer Biol.* **15**, 378–386 (2005).
55. Bashir, S. *et al.* Fundamental Concepts of Hydrogels: Synthesis, Properties, and Their Applications. *Polymers* **12**, 2702 (2020).
56. Reig-Vano, B., Tylkowski, B., Montané, X. & Giamberini, M. Alginate-based hydrogels for cancer therapy and research. *Int. J. Biol. Macromol.* **170**, 424–436 (2021).
57. Grijalvo, S., Nieto-Díaz, M., Maza, R. M., Eritja, R. & Díaz, D. D. Alginate Hydrogels as Scaffolds and Delivery Systems to Repair the Damaged Spinal Cord. *Biotechnol. J.* **14**, 1900275 (2019).
58. Catoira, M. C., Fusaro, L., Di Francesco, D., Ramella, M. & Boccafocchi, F. Overview of natural hydrogels for regenerative medicine applications. *J. Mater. Sci. Mater. Med.* **30**, 115 (2019).

59. Karoyo, A. H. & Wilson, L. D. A Review on the Design and Hydration Properties of Natural Polymer-Based Hydrogels. *Materials* **14**, 1095 (2021).
60. Kozlowski, M. T., Crook, C. J. & Ku, H. T. Towards organoid culture without Matrigel. *Commun. Biol.* **4**, 1–15 (2021).
61. Ho, T.-C. *et al.* Hydrogels: Properties and Applications in Biomedicine. *Molecules* **27**, 2902 (2022).
62. Thakur, S., Thakur, V. K. & Arotiba, O. A. History, Classification, Properties and Application of Hydrogels: An Overview. in *Hydrogels: Recent Advances* (eds. Thakur, V. K. & Thakur, M. K.) 29–50 (Springer, 2018). doi:10.1007/978-981-10-6077-9_2.
63. Madduma-Bandarage, U. S. K. & Madihally, S. V. Synthetic hydrogels: Synthesis, novel trends, and applications. *J. Appl. Polym. Sci.* **138**, 50376 (2021).
64. Dattola, E. *et al.* Development of 3D PVA scaffolds for cardiac tissue engineering and cell screening applications. *RSC Adv.* **9**, 4246–4257 (2019).
65. Shapiro, J. M. & Oyen, M. L. Engineering Approaches for Understanding Osteogenesis: Hydrogels as Synthetic Bone Microenvironments. *Horm. Metab. Res.* **48**, 726–736 (2016).
66. Zhang, H. J. *et al.* Tough Triblock Copolymer Hydrogels with Different Micromorphologies for Medical and Sensory Materials. *ACS Appl. Polym. Mater.* **1**, 1948–1953 (2019).
67. Díaz-Bello, B. *et al.* Method for the Direct Fabrication of Polyacrylamide Hydrogels with Controlled Stiffness in Polystyrene Multiwell Plates for Mechanobiology Assays. *ACS Biomater. Sci. Eng.* **5**, 4219–4227 (2019).
68. Denisin, A. K. & Pruitt, B. L. Tuning the Range of Polyacrylamide Gel Stiffness for Mechanobiology Applications. *ACS Appl. Mater. Interfaces* **8**, 21893–21902 (2016).
69. Tse, J. R. & Engler, A. J. Preparation of Hydrogel Substrates with Tunable Mechanical Properties. *Curr. Protoc. Cell Biol.* **47**, 10.16.1-10.16.16 (2010).

70. Pelham, R. J. & Wang, Y. Cell locomotion and focal adhesions are regulated by substrate flexibility. *Proc. Natl. Acad. Sci. U. S. A.* **94**, 13661–13665 (1997).
71. Thomas, V., Yallapu, M. M., Sreedhar, B. & Bajpai, S. K. A versatile strategy to fabricate hydrogel–silver nanocomposites and investigation of their antimicrobial activity. *J. Colloid Interface Sci.* **315**, 389–395 (2007).
72. Unal, A. Z. & West, J. L. Synthetic ECM: Bioactive Synthetic Hydrogels for 3D Tissue Engineering. *Bioconjug. Chem.* **31**, 2253–2271 (2020).
73. Lin, C.-C. & Metters, A. T. Hydrogels in controlled release formulations: Network design and mathematical modeling. *Adv. Drug Deliv. Rev.* **58**, 1379–1408 (2006).
74. Tang, G. *et al.* Advances of Naturally Derived and Synthetic Hydrogels for Intervertebral Disk Regeneration. *Front. Bioeng. Biotechnol.* **8**, 745 (2020).
75. Kopeček, J. & Yang, J. Smart Self-Assembled Hybrid Hydrogel Biomaterials. *Angew. Chem. Int. Ed Engl.* **51**, 7396–7417 (2012).
76. Vandermeulen, G. W. M. & Klok, H.-A. Peptide/protein hybrid materials: enhanced control of structure and improved performance through conjugation of biological and synthetic polymers. *Macromol. Biosci.* **4**, 383–398 (2004).
77. Wang, C., Stewart, R. J. & Kopeček, J. Hybrid hydrogels assembled from synthetic polymers and coiled-coil protein domains. *Nature* **397**, 417–420 (1999).
78. Ji, Q. *et al.* Hydrosoluble collagen based biodegradable hybrid hydrogel for biomedical scaffold. *J. Biomater. Sci. Polym. Ed.* **31**, 2199–2219 (2020).
79. Samanipour, R. *et al.* Ferritin Nanocage Conjugated Hybrid Hydrogel for Tissue Engineering and Drug Delivery Applications. *ACS Biomater. Sci. Eng.* **6**, 277–287 (2020).
80. Li, X. *et al.* Nanofiber-hydrogel composite–mediated angiogenesis for soft tissue reconstruction. *Sci. Transl. Med.* **11**, eaau6210 (2019).

81. Palmese, L. L., Thapa, R. K., Sullivan, M. O. & Kiick, K. L. Hybrid hydrogels for biomedical applications. *Curr. Opin. Chem. Eng.* **24**, 143–157 (2019).
82. Neves, S. C., Moroni, L., Barrias, C. C. & Granja, P. L. Leveling Up Hydrogels: Hybrid Systems in Tissue Engineering. *Trends Biotechnol.* **38**, 292–315 (2020).
83. Ullah, F., Othman, M. B. H., Javed, F., Ahmad, Z. & Akil, H. Md. Classification, processing and application of hydrogels: A review. *Mater. Sci. Eng. C* **57**, 414–433 (2015).
84. Wang, J., Wei, J., Su, S. & Qiu, J. Tough and Fatigue-Resistant Hydrogels with Triple Interpenetrating Networks. *J. Nanomater.* **2019**, 1–15 (2019).
85. Xu, L. *et al.* Thermosensitive P(AAc-co-NIPAm) Hydrogels Display Enhanced Toughness and Self-Healing via Ion-Ligand Interactions. *Macromol. Rapid Commun.* e2200320 (2022) doi:10.1002/marc.202200320.
86. Çakmak, S., Çakmak, A. S. & Gümüşderelioğlu, M. PNIPAAm-grafted thermoresponsive microcarriers: Surface-initiated ATRP synthesis and characterization. *Mater. Sci. Eng. C* **33**, 3033–3040 (2013).
87. Duan, T., Bian, Q. & Li, H. Light-Responsive Dynamic Protein Hydrogels Based on LOVTRAP. *Langmuir ACS J. Surf. Colloids* **37**, 10214–10222 (2021).
88. Han, X. *et al.* Green and stable piezoresistive pressure sensor based on lignin-silver hybrid nanoparticles/polyvinyl alcohol hydrogel. *Int. J. Biol. Macromol.* **176**, 78–86 (2021).
89. Araújo-Custódio, S. *et al.* Injectable and Magnetic Responsive Hydrogels with Bioinspired Ordered Structures. *ACS Biomater. Sci. Eng.* **5**, 1392–1404 (2019).
90. Huang, J. *et al.* Pulse electromagnetic fields enhance the repair of rabbit articular cartilage defects with magnetic nano-hydrogel. *RSC Adv.* **10**, 541–550 (2020).
91. Walter, S. V., Ennen-Roth, F., Büning, D., Denizer, D. & Ulbricht, M. Glucose-Responsive Polymeric Hydrogel Materials: From a Novel Technique for the Measurement of Glucose Binding toward Swelling Pressure Sensor Applications. *ACS Appl. Bio Mater.* **2**, 2464–2480 (2019).

92. Ghosh, G., Barman, R., Sarkar, J. & Ghosh, S. pH-Responsive Biocompatible Supramolecular Peptide Hydrogel. *J. Phys. Chem. B* **123**, 5909–5915 (2019).
93. Miyata, T., Asami, N. & Urugami, T. A reversibly antigen-responsive hydrogel. *Nature* **399**, 766–769 (1999).
94. Carlini, A. S., Cassidy, M. F. & Gianneschi, N. C. Hydrogel Formation with Enzyme-Responsive Cyclic Peptides. *Methods Mol. Biol. Clifton NJ* **2371**, 427–448 (2022).
95. Lee, W. *et al.* Dispersible hydrogel force sensors reveal patterns of solid mechanical stress in multicellular spheroid cultures. *Nat. Commun.* **10**, 144 (2019).
96. Daly, A. C., Riley, L., Segura, T. & Burdick, J. A. Hydrogel microparticles for biomedical applications. *Nat. Rev. Mater.* **5**, 20–43 (2020).
97. Leong, W., Lau, T. T. & Wang, D.-A. A temperature-cured dissolvable gelatin microsphere-based cell carrier for chondrocyte delivery in a hydrogel scaffolding system. *Acta Biomater.* **9**, 6459–6467 (2013).
98. Xu, Q. *et al.* Preparation of Monodisperse Biodegradable Polymer Microparticles Using a Microfluidic Flow-Focusing Device for Controlled Drug Delivery. *Small* **5**, 1575–1581 (2009).
99. Martín-Banderas, L. *et al.* Flow Focusing: A Versatile Technology to Produce Size-Controlled and Specific-Morphology Microparticles. *Small* **1**, 688–692 (2005).
100. De Geest, B. G., Urbanski, J. P., Thorsen, T., Demeester, J. & De Smedt, S. C. Synthesis of Monodisperse Biodegradable Microgels in Microfluidic Devices. *Langmuir* **21**, 10275–10279 (2005).
101. Forigua, A., Kirsch, R. L., Willerth, S. M. & Elvira, K. S. Recent advances in the design of microfluidic technologies for the manufacture of drug releasing particles. *J. Controlled Release* **333**, 258–268 (2021).
102. Zhu, Z. & Yang, C. J. Hydrogel Droplet Microfluidics for High-Throughput Single Molecule/Cell Analysis. *Acc. Chem. Res.* **50**, 22–31 (2017).

103. Elvira, K. S., Gielen, F., Tsai, S. S. H. & Nightingale, A. M. Materials and methods for droplet microfluidic device fabrication. *Lab. Chip* **22**, 859–875 (2022).
104. Link, A., McGrath, J. S., Zaimagaoglu, M. & Franke, T. Active single cell encapsulation using SAW overcoming the limitations of Poisson distribution. *Lab. Chip* **22**, 193–200 (2021).
105. Abbasi, N., Navi, M., Nunes, J. K. & Tsai, S. S. H. Controlled generation of spiky microparticles by ionic cross-linking within an aqueous two-phase system. *Soft Matter* **15**, 3301–3306 (2019).
106. Bardin, D., Kendall, M. R., Dayton, P. A. & Lee, A. P. Parallel generation of uniform fine droplets at hundreds of kilohertz in a flow-focusing module. *Biomicrofluidics* **7**, 034112 (2013).
107. Shieh, H., Saadatmand, M., Eskandari, M. & Bastani, D. Microfluidic on-chip production of microgels using combined geometries. *Sci. Rep.* **11**, 1565 (2021).
108. Laza, S. C. *et al.* Two-Photon Continuous Flow Lithography. *Adv. Mater.* **24**, 1304–1308 (2012).
109. Helgeson, M. E., Chapin, S. C. & Doyle, P. S. Hydrogel microparticles from lithographic processes: novel materials for fundamental and applied colloid science. *Curr. Opin. Colloid Interface Sci.* **16**, 106–117 (2011).
110. Liu, X. *et al.* Fabrication and Characterization of Reconstituted Silk Microgels for the Storage and Release of Small Molecules. *Macromol. Rapid Commun.* **40**, e1800898 (2019).
111. Imaninezhad, M., Jain, E. & Zustiak, S. P. Cell Microencapsulation in Polyethylene Glycol Hydrogel Microspheres Using Electrohydrodynamic Spraying. in *Organoids: Stem Cells, Structure, and Function* (ed. Turksen, K.) 313–325 (Springer, 2019). doi:10.1007/7651_2017_58.
112. Gansau, J., Kelly, L. & Buckley, C. T. Influence of key processing parameters and seeding density effects of microencapsulated chondrocytes fabricated using electrohydrodynamic spraying. *Biofabrication* **10**, 035011 (2018).
113. Jeyhani, M. *et al.* Controlled Electrospray Generation of Nonspherical Alginate Microparticles. *ChemPhysChem* **19**, 2113–2118 (2018).

114. Qayyum, A. S. *et al.* Design of electrohydrodynamic sprayed polyethylene glycol hydrogel microspheres for cell encapsulation. *Biofabrication* **9**, 025019 (2017).
115. Hinton, T. J. *et al.* Three-dimensional printing of complex biological structures by freeform reversible embedding of suspended hydrogels. *Sci. Adv.* **1**, e1500758 (2015).
116. Sinclair, A. *et al.* Self-Healing Zwitterionic Microgels as a Versatile Platform for Malleable Cell Constructs and Injectable Therapies. *Adv. Mater. Deerfield Beach Fla* **30**, e1803087 (2018).
117. Muir, V. G., Qazi, T. H., Shan, J., Groll, J. & Burdick, J. A. Influence of Microgel Fabrication Technique on Granular Hydrogel Properties. *ACS Biomater. Sci. Eng.* **7**, 4269–4281 (2021).
118. Qazi, T. H., Muir, V. G. & Burdick, J. A. Methods to Characterize Granular Hydrogel Rheological Properties, Porosity, and Cell Invasion. *ACS Biomater. Sci. Eng.* **8**, 1427–1442 (2022).
119. Feig, V. R. *et al.* Conducting polymer-based granular hydrogels for injectable 3D cell scaffolds. *Adv. Mater. Technol.* **6**, 2100162 (2021).
120. Muir, V. G. *et al.* Sticking Together: Injectable Granular Hydrogels with Increased Functionality via Dynamic Covalent Inter-Particle Crosslinking. *Small* **18**, 2201115 (2022).
121. Jin, Y., Compaan, A., Bhattacharjee, T. & Huang, Y. Granular gel support-enabled extrusion of three-dimensional alginate and cellular structures. *Biofabrication* **8**, 025016 (2016).
122. Fang, J. *et al.* Injectable Drug-Releasing Microporous Annealed Particle Scaffolds for Treating Myocardial Infarction. *Adv. Funct. Mater.* **30**, 2004307 (2020).
123. Griffin, D. R., Weaver, W. M., Scumpia, P. O., Di Carlo, D. & Segura, T. Accelerated wound healing by injectable microporous gel scaffolds assembled from annealed building blocks. *Nat. Mater.* **14**, 737–744 (2015).
124. Caldwell, A. S., Campbell, G. T., Shekiri, K. M. T. & Anseth, K. S. Clickable Microgel Scaffolds as Platforms for 3D Cell Encapsulation. *Adv. Healthc. Mater.* **6**, 1700254 (2017).

125. Truong, N. F. *et al.* Microporous annealed particle hydrogel stiffness, void space size, and adhesion properties impact cell proliferation, cell spreading, and gene transfer. *Acta Biomater.* **94**, 160–172 (2019).
126. Sideris, E. *et al.* Particle Hydrogels Based on Hyaluronic Acid Building Blocks. *ACS Biomater. Sci. Eng.* **2**, 2034–2041 (2016).
127. Nih, L. R., Sideris, E., Carmichael, S. T. & Segura, T. Injection of Microporous Annealing Particle (MAP) Hydrogels in the Stroke Cavity Reduces Gliosis and Inflammation and Promotes NPC Migration to the Lesion. *Adv. Mater.* **29**, 1606471 (2017).
128. Costa, S. A. *et al.* Photo-Crosslinkable Unnatural Amino Acids Enable Facile Synthesis of Thermoresponsive Nano- to Microgels of Intrinsically Disordered Polypeptides. *Adv. Mater. Deerfield Beach Fla* **30**, (2018).
129. Riley, L., Schirmer, L. & Segura, T. Granular hydrogels: emergent properties of jammed hydrogel microparticles and their applications in tissue repair and regeneration. *Curr. Opin. Biotechnol.* **60**, 1–8 (2019).
130. Wyss, C. S., Karami, P., Bourban, P.-E. & Pioletti, D. P. Hybrid granular hydrogels: combining composites and microgels for extended ranges of material properties. *Soft Matter* **16**, 3769–3778 (2020).
131. Kessler, M., Nassisi, Q. & Amstad, E. Does the Size of Microgels Influence the Toughness of Microgel-Reinforced Hydrogels? *Macromol. Rapid Commun.* **43**, 2200196 (2022).
132. Charlet, A., Bono, F. & Amstad, E. Mechanical reinforcement of granular hydrogels. *Chem. Sci.* **13**, 3082–3093 (2022).
133. Du, H., Cont, A., Steinacher, M. & Amstad, E. Fabrication of Hexagonal-Prismatic Granular Hydrogel Sheets. *Langmuir ACS J. Surf. Colloids* **34**, 3459–3466 (2018).
134. Rao, V. V. *et al.* Granular PEG hydrogels mediate osteoporotic MSC clustering via N-cadherin influencing the pro-resorptive bias of their secretory profile. *Acta Biomater.* **145**, 77–87 (2022).

135. Chen, Y. *et al.* Structural characterization and statistical properties of jammed soft ellipsoid packing. *Soft Matter* **17**, 2963–2972 (2021).
136. Caldwell, A. S. *et al.* Mesenchymal stem cell-inspired microgel scaffolds to control macrophage polarization. *Bioeng. Transl. Med.* **6**, e10217 (2021).
137. Sakthivel, K. *et al.* High Throughput Screening of Cell Mechanical Response Using a Stretchable 3D Cellular Microarray Platform. *Small* **16**, 2000941 (2020).
138. Mahdieh, Z. *et al.* Granular Matrigel: restructuring a trusted extracellular matrix material for improved permeability. *Biomed. Mater.* **17**, 045020 (2022).
139. Wagner, K. *et al.* Colloidal crystals of compliant microgel beads to study cell migration and mechanosensitivity in 3D. *Soft Matter* **15**, 9776–9787 (2019).
140. Pruett, L. J., Taing, A. L., Singh, N. S., Peirce, S. M. & Griffin, D. R. In silico optimization of heparin microislands in microporous annealed particle hydrogel for endothelial cell migration. *Acta Biomater.* **148**, 171–180 (2022).
141. Zhang, L. *et al.* Solid multifunctional granular bioink for constructing chondroid basing on stem cell spheroids and chondrocytes. *Biofabrication* **14**, 035003 (2022).
142. Tonelli, A. E., Narayanan, G. & Gurarslan, A. Host–Guest Polymer Complexes. *Polymers* **10**, 911 (2018).
143. Sayed, M. & Pal, H. An overview from simple host–guest systems to progressively complex supramolecular assemblies. *Phys. Chem. Chem. Phys.* **23**, 26085–26107 (2021).
144. Madl, A. C. & Myung, D. Supramolecular Host–Guest Hydrogels for Corneal Regeneration. *Gels* **7**, 163 (2021).
145. Ni, Y. *et al.* Host–Guest Interaction-Mediated Photo/Temperature Dual-Controlled Antibacterial Surfaces. *ACS Appl. Mater. Interfaces* **13**, 14543–14551 (2021).
146. Wu, H. *et al.* An Activatable Host–Guest Conjugate as a Nanocarrier for Effective Drug Release through Self-Inclusion. *ACS Appl. Mater. Interfaces* **13**, 33962–33968 (2021).

147. Wang, X. *et al.* Chiroptical Sensing of Amino Acid Derivatives by Host–Guest Complexation with Cyclo[6]aramide. *Molecules* **26**, 4064 (2021).
148. Dan, Z. *et al.* A pH-Responsive Host-guest Nanosystem Loading Succinobucol Suppresses Lung Metastasis of Breast Cancer. *Theranostics* **6**, 435–445 (2016).
149. Mukhopadhyay, R. D., Das, G. & Ajayaghosh, A. Stepwise control of host–guest interaction using a coordination polymer gel. *Nat. Commun.* **9**, 1987 (2018).
150. Bian, Q. *et al.* Host-guest self-assembly toward reversible visible-light-responsive switching for bacterial adhesion. *Acta Biomater.* **76**, 39–45 (2018).
151. Kang, Y. *et al.* An Amylase-Responsive Bolaform Supra-Amphiphile. *ACS Appl. Mater. Interfaces* **8**, 4927–4933 (2016).
152. Yu, Q., Zhang, Y.-M., Liu, Y.-H., Xu, X. & Liu, Y. Magnetism and photo dual-controlled supramolecular assembly for suppression of tumor invasion and metastasis. *Sci. Adv.* **4**, eaat2297 (2018).
153. Tang, J.-H. *et al.* Single-molecule level control of host-guest interactions in metallocycle-C60 complexes. *Nat. Commun.* **10**, 4599 (2019).
154. Sugawara, A., Asoh, T.-A., Takashima, Y., Harada, A. & Uyama, H. Mechano-Responsive Hydrogels Driven by the Dissociation of a Host-Guest Complex. *ACS Macro Lett.* **10**, 971–977 (2021).
155. Tsuchiya, H. *et al.* Supramolecular Biocomposite Hydrogels Formed by Cellulose and Host–Guest Polymers Assisted by Calcium Ion Complexes. *Biomacromolecules* **21**, 3936–3944 (2020).
156. Kakuta, T., Takashima, Y. & Harada, A. Highly Elastic Supramolecular Hydrogels Using Host–Guest Inclusion Complexes with Cyclodextrins. *Macromolecules* **46**, 4575–4579 (2013).
157. Ren, Z., Ke, T., Ling, Q., Zhao, L. & Gu, H. Rapid self-healing and self-adhesive chitosan-based hydrogels by host-guest interaction and dynamic covalent bond as flexible sensor. *Carbohydr. Polym.* **273**, 118533 (2021).

158. Wang, Z. *et al.* 3D-printable self-healing and mechanically reinforced hydrogels with host-guest non-covalent interactions integrated into covalently linked networks. *Mater. Horiz.* **6**, 733–742 (2019).
159. Schindelin, J. *et al.* Fiji: an open-source platform for biological-image analysis. *Nat. Methods* **9**, 676–682 (2012).
160. Mok, S. *et al.* Mapping cellular-scale internal mechanics in 3D tissues with thermally responsive hydrogel probes. *Nat. Commun.* **11**, 1–11 (2020).

10 Appendix 1: Supplementary Material

10.1 Initial Ad and β CD concentration curves

Initial curves were created to characterize the functionalization of PAAm beads with Ad or β CD. These curves helped inform later decisions of guest and host functionalization amounts by recognizing plateaus in normalized intensity. That is, an upper limit to PAAm bead functionalization were increasing the concentration of Ad-AAm or β CD-AAm in the pre-gel set up did not increase the functionality of the beads. It was seen between 2 and 4 mg/ml of Ad in the kerosene phase, and somewhere after 10 mg/ml to 24 mg/ml of β CD in the pre-gel.

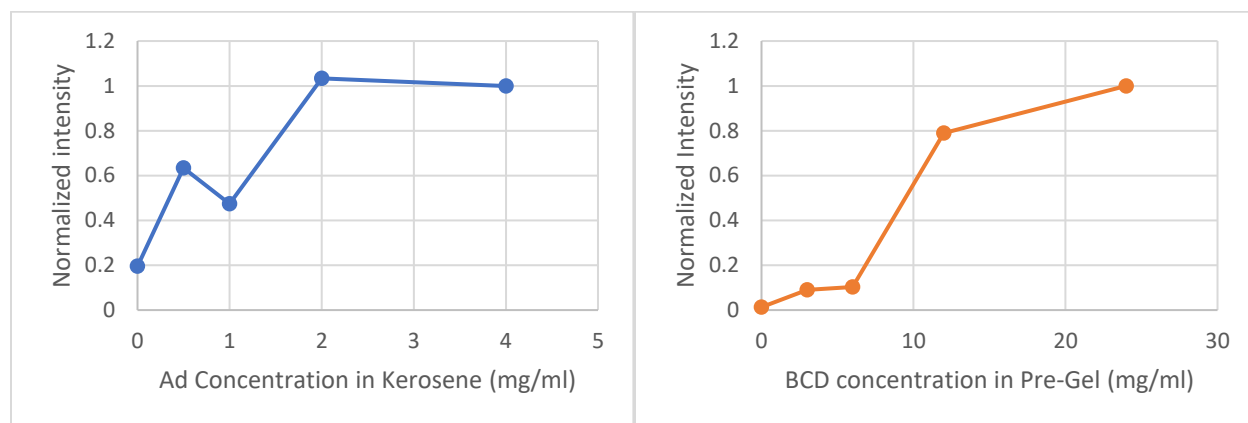


Figure 23: Initial fluorescent guest host functionalization curves for Ad and β CD.